Technical Report
TR-17-04
May 2018

Buffer homogenisation – status report 4

Ann Dueck
Reza Goudarzi
Lennart Börgesson

SVENSK KÄRNBRÄNSLEHANTERING AB

SWEDISH NUCLEAR FUEL
AND WASTE MANAGEMENT CO

Box 3091, SE-169 03 Solna
Phone +46 8 459 84 00
skb.se

SVENSK KÄRNBRÄNSLEHANTERING

ISSN 1404-0344
SKB TR-17-04
ID 1579254
May 2018

Buffer homogenisation – status report 4

Ann Dueck, Reza Goudarzi, Lennart Börgesson
Clay Technology AB

Keywords: Bentonite, Swelling, Swelling pressure, Homogenisation.

Abstract

The present status report is a compilation of laboratory test results from a project on homogenisation tests of bentonite. The main purpose of the status report is to account for results derived up to July 2016 and to provide results that can be used for modelling some well-defined benchmark tests in order to improve the models or determine mechanical parameters for thermo-hydro-mechanical modelling of the behaviour of the bentonite buffer. Further analyses of the tests, test conditions, test results and limitations of the results will be made later in the project.

Results from supplementary fundamental swelling tests with different water supply and tests on friction between confined bentonite specimens and different types of surfaces are presented in this status report. Buffer homogenisation has also been studied by medium scale tests involving loss of bentonite and the results from the second one now finished is presented in this report. Remaining differences of density after long time is studied in a series with long tubes. One of ten tests of this type has been dismantled and is reported.

Sammanfattning

Denna lägesrapport innehåller en sammanställning av laboratorieförsök som utförts för att studera homogeniseringsprocessen i bentonitlera. Huvudsyftet med rapporten är att presentera försöksresultat från försök som utförts fram till och med juli 2016 och att tillhandahålla resultat som kan användas för modellering, för att förbättra modeller eller för att bestämma mekaniska parametrar för den termo-hydro-mekaniska modelleringen av bentonitbuffertens uppförande. Analys av försöken, förutsättningar, försöksresultat och begränsningar i försöken kommer att göras senare i projektet.

Resultat från kompletterande svällningsförsök med olika vattentillförsel och försök som undersöker friktionen mellan bentonit och andra ytor presenteras i denna statusrapport. Bufferthomogenisering har i detta projekt också undersökts med så kallade självläkningsförsök där effekten av förlust av bentonitmaterial har studerats och resultatet från det andra försöket av denna typ presenteras i denna rapport. Skillnader i densitet som kvarstår efter lång tid har studerats i en serie försök med så kallat långa rör. Ett av tio försök av denna typ har avslutats och resultatet presenteras här.

Contents

1 Introduction

1.1 Background

Swelling of the buffer blocks and buffer homogenisation are important functions to guarantee the requirements of the buffer in a deposition hole after full water saturation. It is important to understand and be able to predict the final condition of the buffer after the swelling and homogenisation, which occur both during the initial saturation phase and after possible loss of bentonite caused by for example erosion.

The project consists of four parts; theoretical studies, fundamental laboratory tests, laboratory study of the influence of friction and medium scale tests of the scenario involving loss of bentonite. The present status report describes results from all of the mentioned laboratory tests.

The tests described were run from July 2014 and until July 2016. This is the forth status report from the actual project and it is a continuation of the previous status reports with laboratory test results Dueck et al. (2011, 2014, 2016). In addition, material models have been developed and verified with some of the laboratory test results from this project.

1.2 Objective

The objective of the described tests has been to further improve the knowledge of the process of swelling and buffer homogenisation. The main purpose of this status report is to account for results derived up to July 2016 and provide results that can be used for modelling some well-defined benchmark tests in order to improve the models or determine mechanical parameters for thermo-hydro-mechanical modelling of the behaviour of the buffer.

1.3 Content of the report

The determination of base variables is described in Chapter 2 and the materials used for the tests are described in Chapter 3. In Chapter 4 the test techniques and the results from fundamental swelling tests in the so called high resolution series and from the series with measurement of friction between bentonite and other surfaces are presented. In Chapter 4 the test technique and the results from a series with so called wetting tests are also presented. Chapter 5 contains test description and results from the second of two now completed and dismantled medium scale tests of a scenario involving loss of bentonite. In Chapter 6 the test type with the so called long tubes is described together with the results from one completed and dismantled specimen and the status of the other nine still ongoing. In addition, results are also presented in Appendix 1–5 and in Appendix 6 a tabulated compilation of specimens presented in this and the two previous reports is shown.

Some of the tests run in this project were used as tasks or used as background material in the SKB project Task Force on Engineered Barriers (TF EBS) and Chapter 5 was used in full with the title: *PM – Preparation and dismantling of SH1. Buffer homogenisation after loss of bentonite – medium scale laboratory test*.

Short comments about the test results are given directly after each section with presented results. Since the present report is a status report analyses and conclusions of the test results will be provided in a coming report from this project.

2 Determination of basic variables

2.1 General

The basic variables water content and bulk density are measured in each test and from those variables the dry density and degree of saturation are calculated. The swelling pressure is in this project measured as a stress exerted as a load on a piston with a certain area. In most of the tests the measurement is made in a specified direction; i.e. as an axial stress or a radial stress.

2.2 Water content and bulk density determination

The basic geotechnical variables water content w (%), void ratio e, degree of saturation S_r (%) and dry density ρ_d (kg/m^3) are determined according to Equations 2-1 to 2-4.

$$w = 100 \cdot \frac{m_{tot} - m_s}{m_s} \qquad \text{(Equation 2-1)}$$

$$e = \frac{\rho_s}{\rho}(1 + w/100) - 1 \qquad \text{(Equation 2-2)}$$

$$S_r = \frac{\rho_s \cdot w}{\rho_w \cdot e} \qquad \text{(Equation 2-3)}$$

$$\rho_d = \frac{m_s}{V} \qquad \text{(Equation 2-4)}$$

where

m_{tot} = total mass of the specimen (kg)

m_s = dry mass of the specimen (kg)

ρ_s = particle density (kg/m^3)

ρ_w = density of water (kg/m^3)

ρ = bulk density of the specimen (kg/m^3)

V = total volume of the specimen (m^3)

The dry mass of a specimen is obtained from drying a wet specimen at 105 °C for 24h. The bulk density is calculated from the total mass of a specimen and the volume determined by weighing the specimen above and submerged into paraffin oil.

3 Materials

3.1 General

Two bentonite materials have been used; the commercial Wyoming bentonite with brand name Volclay MX-80 from American Coll. Co. and the commercial bentonite Calcigel from Clariant (Süd-Chemie AG). Descriptions of the materials and basic variables were presented by Svensson et al. (2011).

The bentonite powder was delivered with an approximate water content of 10 %. For tests where higher initial water content was used the powder was mixed with de-ionized water. Blocks were made by compacted powder either by compaction directly to the intended size or by sawing from larger compacted blocks.

For determination of void ratio and degree of saturation the particle densities ρ_s = 2 780 kg/m^3 and ρ_s = 2 695 kg/m^3 were used for MX-80 and Calcigel, respectively (Svensson et al. 2011) and the water density ρ_w = 1 000 kg/m^3.

The majority of the tests were supplied with de-ionized stagnant water if nothing else is specified. However, in many tests the filters were flushed in order to get rid of air bubbles.

3.2 Characterisation

The material used, i.e. MX-80 and Calcigel, have been characterized by determination of particle density, swell index, liquid limit and CEC according to the description by Johannesson (2014). The results are shown in Table 3-1. There is a scatter in the determined values of particle density but the values mentioned above, Section 3.1, were used for the calculations in this report. Swelling pressure measured at constant volume conditions has in this project been determined only on reference specimens of MX-80, Figure 3-1.

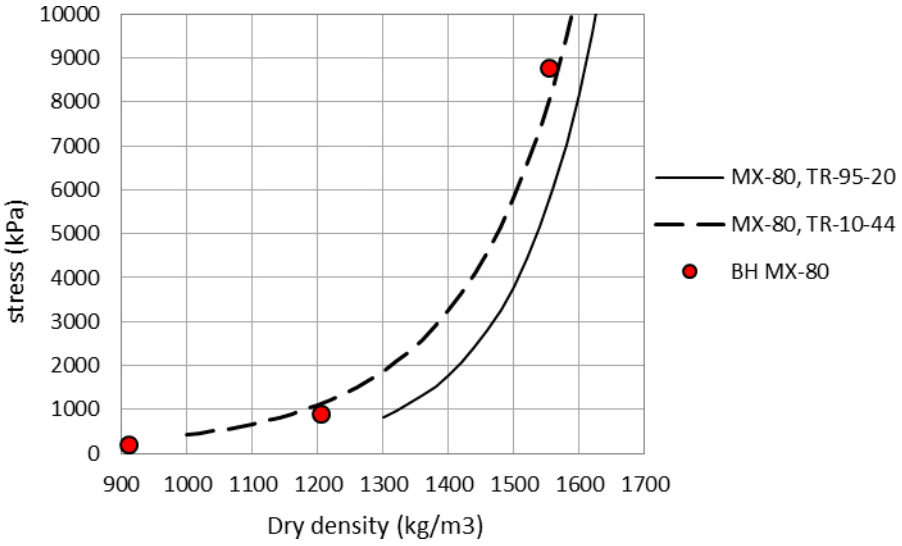

Figure 3-1. *Swelling pressure as a function of density of MX-80; three specimens from this study (label BH MX-80) with models of MX-80 presented by Börgesson et al. (1995) and Åkesson et al. (2010).*

Table 3-1. Characterisation of the materials MX-80 and Calcigel used in the project.

Material ID	Material	Particle density		Swell index		Liquid limit		Cation exchange capacity		Remarks previous name
		ρ_s kg/m^3	no.[2]	V_w %	no.[2]	w_L ml	no.[2]	CEC meq/100 g	no.[2]	
MX-80 #2010[b]	MX-80	2 749	7	19	2	493	1	85.34	2	MX-80 #BH1[1]
MX-80 #2012	MX-80	2 767	2	16	2	488	1	87.94	2	MX-80 2012#5
Calcigel #2006	Calcigel	2 729	7	3	2	111	1	71.07	2	Calcigel 2006#2
Calcigel #2014	Calcigel	2 697	2	4	2	129	1			Calcigel 2014#2

[1] Additional name is MX-80 2010–2013.

[2] Number of tests.

4 Fundamental swelling tests and measurements of friction

4.1 General

In this chapter results from three different test series are presented. Results from supplementary tests from two series; the fundamental swelling tests in the so called HR-series and the measurements of friction in the Fr-series, are presented with results from the so called Wetting tests in the W-series.

The test techniques used in the first two test series have been reported in the previous status reports of this project (Dueck et al. 2011, 2014, 2016) and are only briefly described below. The third test series has not been mentioned earlier.

4.2 Fundamental swelling tests – high resolution series

Fundamental swelling tests have been performed in two scales within the project; the basic series and the series with larger specimens, the so called high resolution series (HR). In this chapter only test results from the supplementary tests of the latter series are presented. Additional results can be found in Appendix 1.

Test description

In the HR-series three types of swelling were studied; axial swelling (HR-A), radial outward swelling (HR-Ro) and radial inward swelling (HR-Ri). Sketches of the set-up used for the tests are shown in Figure 4-1. The tests were done with a free swelling surface, i.e. no counteracting force until the swelling bentonite gel had reached the outer limited surface. In all tests the friction was minimized by use of a mineral-oil based lubricant on relevant surfaces.

In the HR-series the initial degree of saturation was high and for that reason the swelling phase started directly, i.e. no saturation took place in the test devices before the swelling phase. The specimens were sawn and trimmed from larger blocks with the initial water content between 20 % and 24 %. The initial height and diameter of the specimens swelling axially were 40–50 mm and 100 mm, respectively. The specimens swelling radially had the initial height and outer diameter 80 mm and 80–97 mm, respectively.

After preparation the specimens were mounted into the actual device, the load cells were fixed at their positions and de-ionized water was applied to the filters after air evacuation of the filters and tubes. Water was only added to the upper part of the specimen at axial swelling, only added to the radial filter at radial outward swelling and at the radial inward swelling added to the radial filter and also filled into the cavity.

The movable piston and the load cell used for the radially measured swelling pressure were in some tests initially fixed to their positions by applying a small pre-stress illustrated to the left in Figure 4-2. Since this pre-stress is applied to the test equipment and not to the bentonite surface it has to be exceeded by the swelling pressure before the measured stress is representative of the test conditions shown to the right in Figure 4-2.

In the final part of the HR-tests presented in this report water pressure was applied to study the effect on the measured stresses, on the final swelling pressures and if possible also on the density gradients after dismantling. The water pressure was then adjusted back to zero and when no or negligibly small changes were noticed in the measured stresses the homogenisation was considered as completed. Finally, the specimens were dismantled and cut in slices for the determination of water content and density distribution in the direction of swelling.

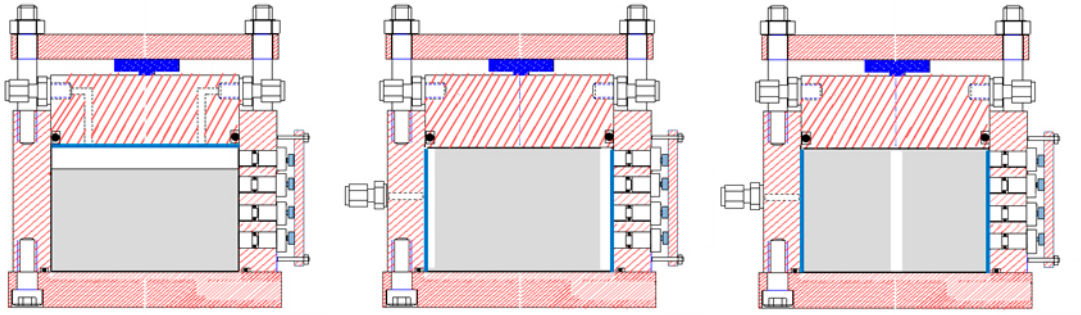

Figure 4-1. *Sketches of the test equipment used for the tests in the HR-series; axial swelling (left), radial outward swelling (middle), radial inward swelling (right).*

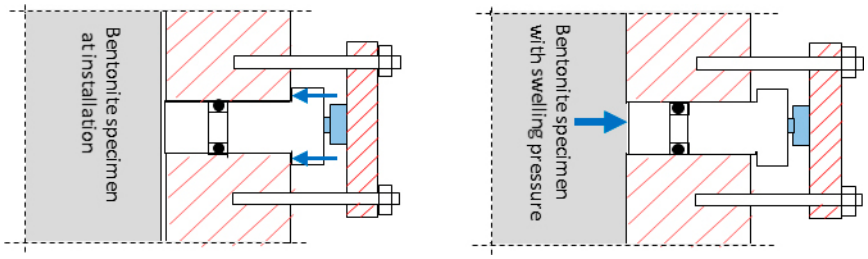

Figure 4-2. *Details of the movable piston and load cell used for radially measured swelling pressure where the pre-stress (to the left) and the bentonite swelling pressure (to the right) are illustrated. The displacement of the piston is exaggerated to illustrate.*

Results (HR-series)

In the test series with HR-tests the following tests were performed and presented in this report. Only four new tests have been completed in the series and the results are presented with initial and final values of w and ρ_d as a function of the specimen height (series HR-A) or radius (series HR-Ro and HR-Ri), i.e. as distribution in the direction of swelling. The evolution of the swelling pressure measured as stress in different directions is then presented with time and finally the stresses are presented together with previous results from this project.

Table 4.1. Tests run in the high resolution series and presented in this report.

Specimen	Type of swelling	Material
HR-A7, HR-A8	Axial swelling	Calcigel
HR-Ro3	Radial outward swelling	Calcigel
HR-Ri2	Radial inward swelling	Calcigel

The term swelling pressure is determined as an axial stress P_{axial} or a radial stress P_{radial} exerted as loads on a piston with a certain area, see Section 2.1. In some tests when a water pressure, P_w, is applied the results are given as an effective stress calculated as the total measured stress minus the water pressure; $P_{axial} - P_w$ or $P_{radial} - P_w$. In some results the stresses are given as an average stress which is then calculated according to Equation 4-1.

$$P_{average} = (P_{axial} + 2 \times P_{radial})/3 \qquad \text{(Equation 4-1)}$$

The measured stresses are shown and compared with models of swelling pressure of MX-80 presented by Börgesson et al. (1995) and by Åkesson et al. (2010) where the latter model was based on results presented by Karnland et al. (2006).

The labels in the diagrams give information about the specimen ID, which includes the type of swelling; HR-A, HR-Ro or HR-Ri (axial swelling, radial outward swelling or radial inward swelling). In most of the labels the swelling is given in % but in some of the labels, used for measured stresses, the position of the measurement is given instead and then as a distance in mm from the bottom of the specimen. The swelling is calculated according to Equation 4-2 where V_i, V_f, ρ_{di} and ρ_{df} are the initial volume, final volume, initial dry density and final dry density, respectively.

$$s = \frac{\Delta V}{V_i} = \frac{V_f}{V_i} - 1 = \frac{\rho_{di}}{\rho_{df}} - 1 \qquad \text{(Equation 4-2)}$$

For the tests involving radial swelling the water content and density distribution after completed swelling were measured by dividing the central part of the specimen in 5 mm pieces as shown in Figure 4-3 (to the left). It is desired to have the sampling done so that the density distribution could be plotted as a function of the radius but since this would give too small samples close to the centre, the sampling had to be done as shown in the figure. The results from each sample are therefore presented as a function of a radius r_c, calculated according to Equation 4-3, instead of as a function of the radius r_a measured along the x-axis, see Figure 4-3 (to the right). This is done to take the actual sampling geometry into account.

$$r_c = (r_a^2 + (L/4)^2)^{0.5} \qquad \text{(Equation 4-3)}$$

Axial swelling

The completed tests of axial swelling are presented in Table 4-2. The test HR-A8 was made with two initial densities put together which means that there was no swelling. In Figure 4-4, Figure 4-5 and Figure 4-6 the distributions of water content w, dry density ρ_d and degree of saturation S_r, respectively, measured after completed tests are shown. The evolution of the stresses measured during the tests are shown in Figure 4-7 to Figure 4-10 where the results from the last time period of the tests, when water pressure was applied are shown separately. In order to investigate the influence of water pressure 500 kPa was applied on HR-A7 and 100 kPa on HR-A8 for a couple of weeks. In Figure 4-7 the initial stresses radially measured, at 45 mm and 60 mm from the bottom, of about 60 kPa were caused by the pre-stress mentioned above. In Figure 4-11 the axially and radially measured stresses are plotted as a function of dry density to the left. To the right the corresponding average stresses are shown together with comparable specimens of Calcigel presented in previous reports in this project; HR-A6, A04-1 and A04-2.

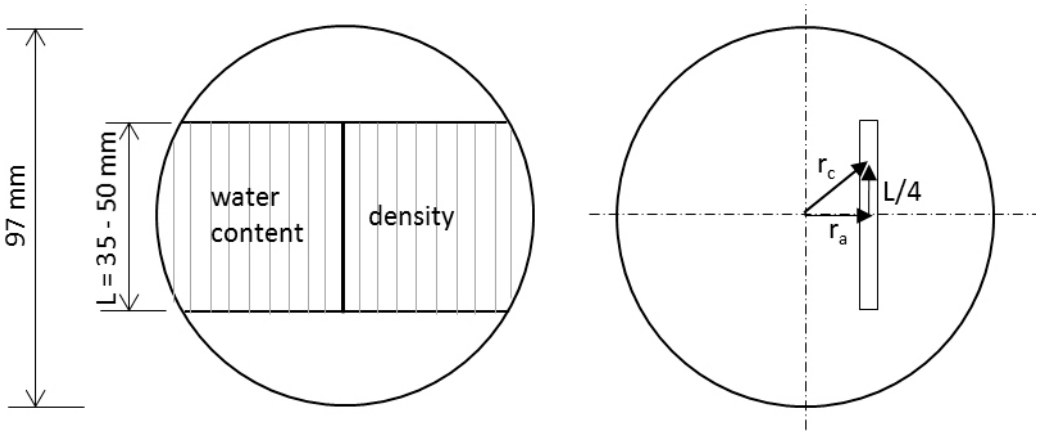

Figure 4-3. *Sampling scheme for the HR-R tests (left). Calculation of the corrected radius r_c of the sampling (right). The distance L is equal to 50 mm and 35 mm in the tests HR-Ro and HR-Ri, respectively.*

Table 4-2. Specimens used in the series with axial swelling, HR-A. The swelling (%) was calculated according to Equation 4-2.

Test ID	Material	Initial water content %	Initial dry density kg/m³	Initial degree of saturation	Constant diameter mm	Initial height mm	Final height mm	Final swelling %
HR-A7	Calcigel	20	1644[1]	84	100	50	70	39
HR-A8	Calcigel	22	1169[2]	93[2]	100	70	70	0

[1] Compacted to initial dry density 1730 kg/m³ but with the diameter 97.5 mm. [2] Compacted in two pieces with different dry densities; 1407 and 932 kg/m³. The given value is the average.

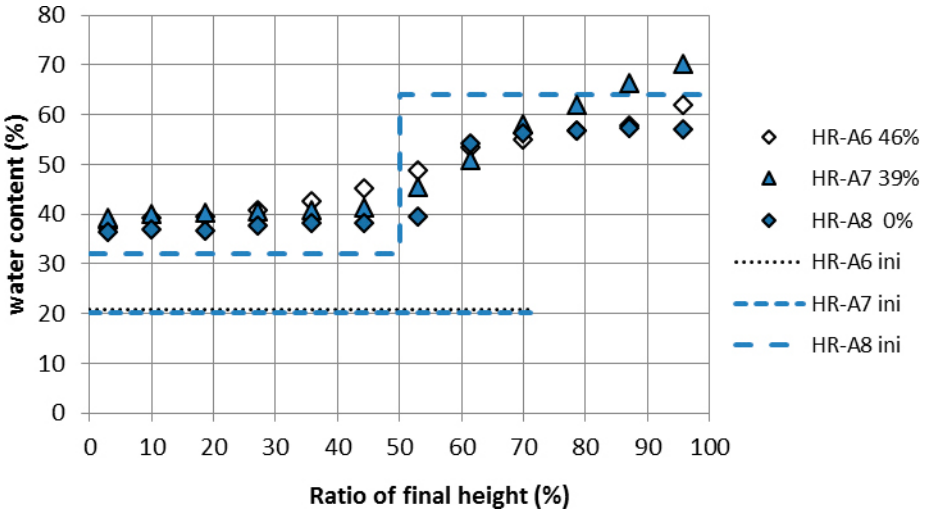

Figure 4-4. Distribution of water content over the height of specimens HR-A7 and HR-A8. In addition results of HR-A6 (open symbols) from Dueck et al. (2016).

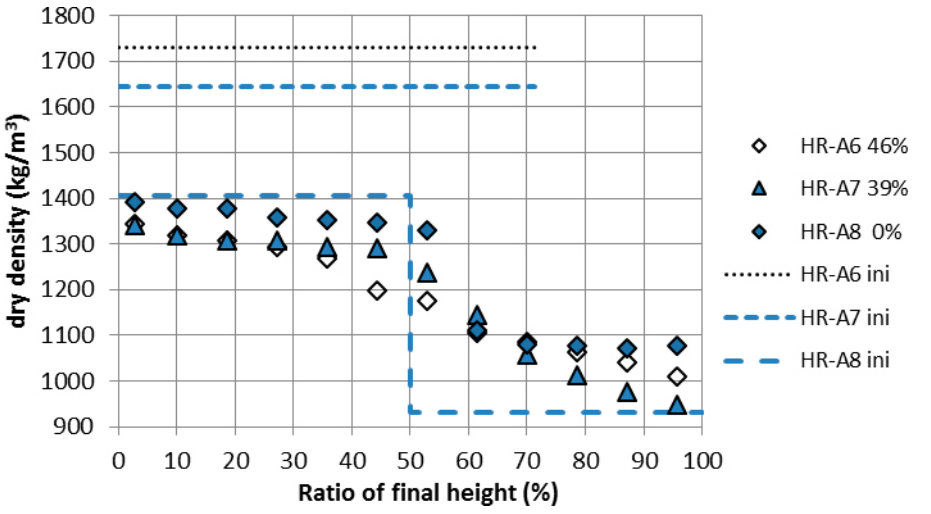

Figure 4-5. Distribution of dry density over the height of specimens HR-A7 and HR-A8. In addition results of HR-A6 (open symbols) from Dueck et al. (2016).

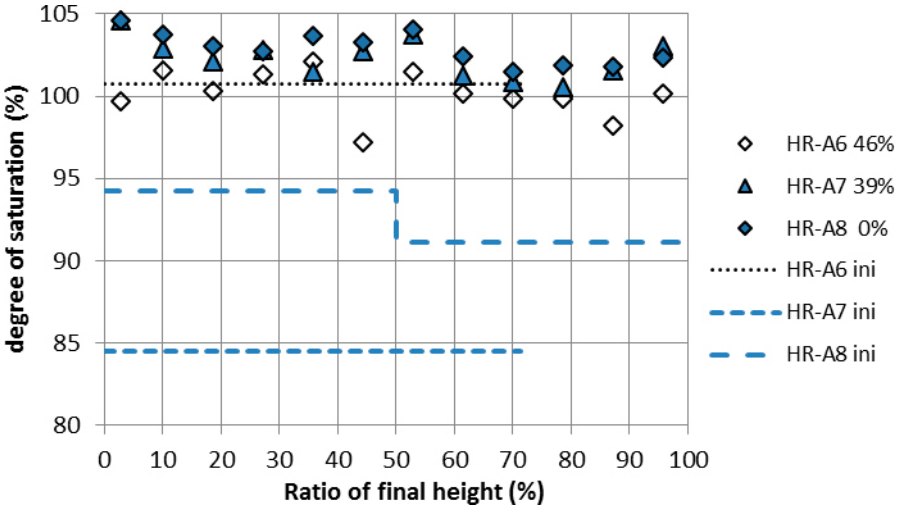

Figure 4-6. *Distribution of degree of saturation over the height of specimens HR-A7 and HR-A8, calculated with ρ_s = 2 695 kg/m³, see also the section with Comments. In addition results of HR-A6 (open symbols) from Dueck et al. (2016).*

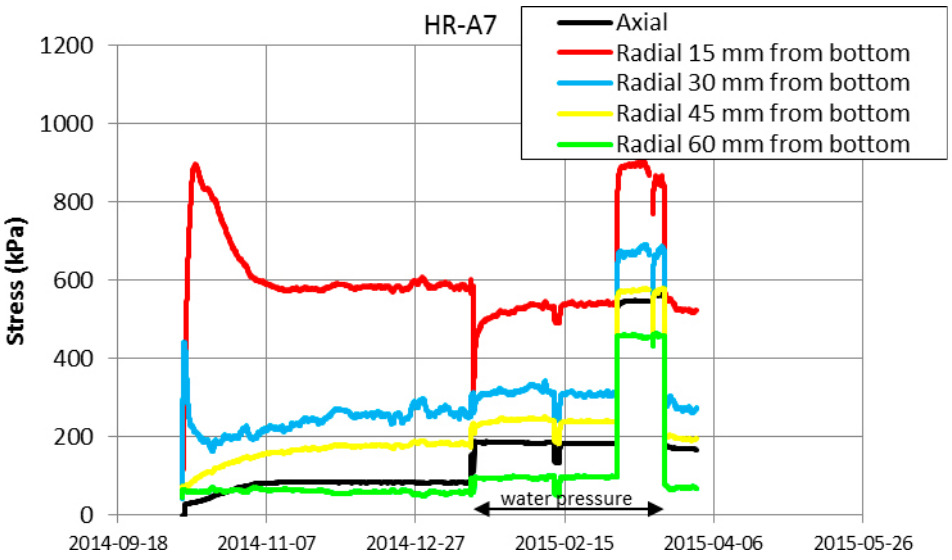

Figure 4-7. *Evolution of total stress with time, HR-A7.*

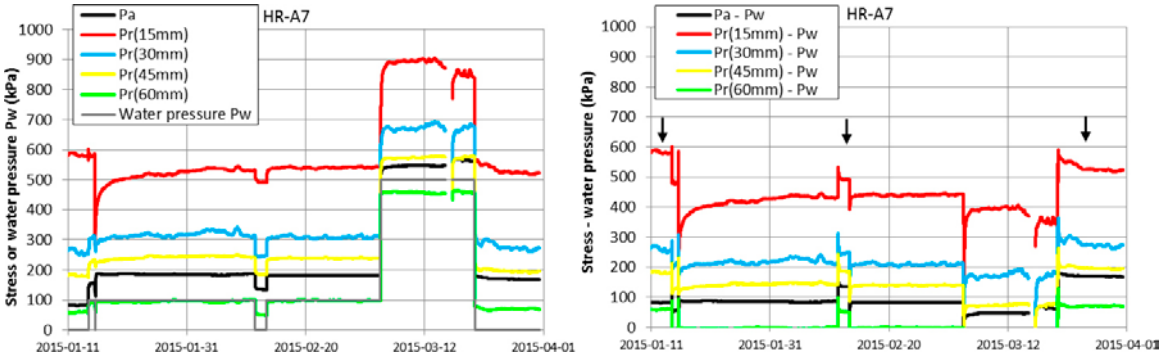

Figure 4-8. *Stress and pressure as a function of time from the last four months of HR-A7. The measured stresses plotted with the applied water pressure (to the left) and the effective stress, calculated as total stress minus water pressure, (to the right). The arrows mark the stresses measured at zero water pressure.*

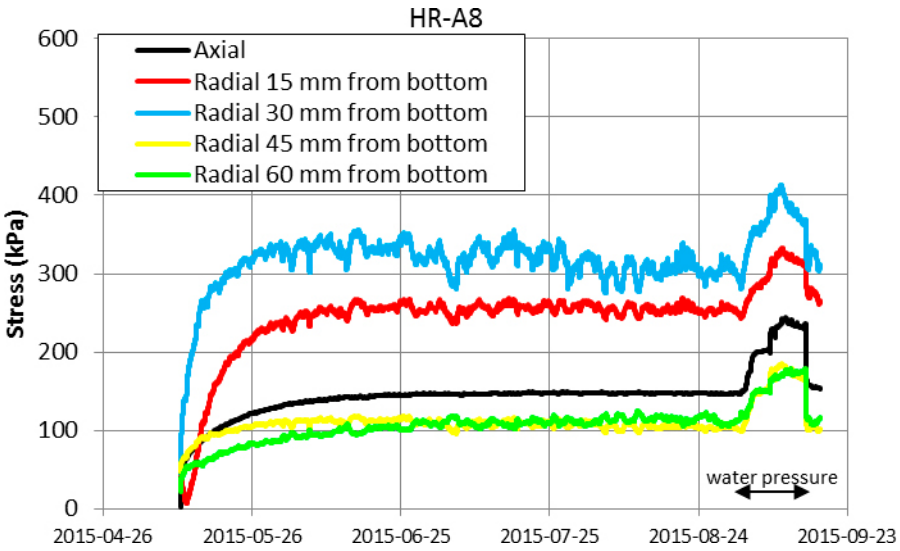

Figure 4-9. *Evolution of total stress with time, HR-A8.*

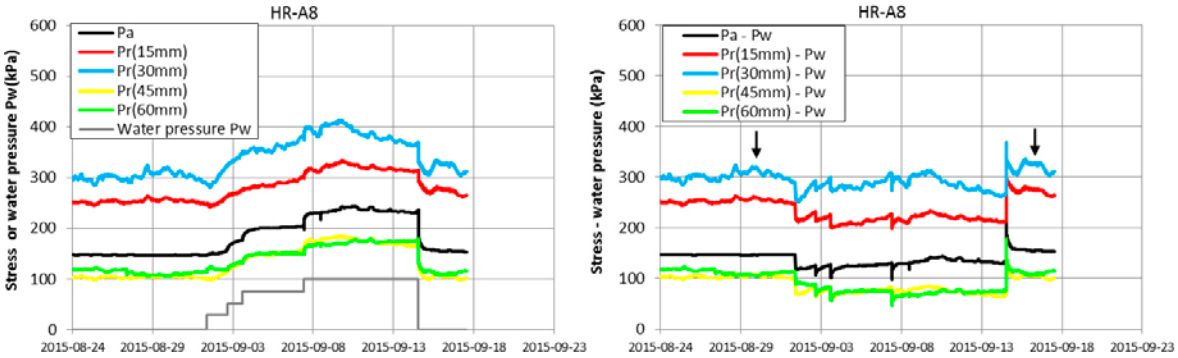

Figure 4-10. *Stress and pressure as a function of time from the last month of HR-A8. The measured stresses plotted with the applied water pressure (to the left) and the effective stress, calculated as total stress minus water pressure (to the right). The arrows mark the stresses measured at zero water pressure.*

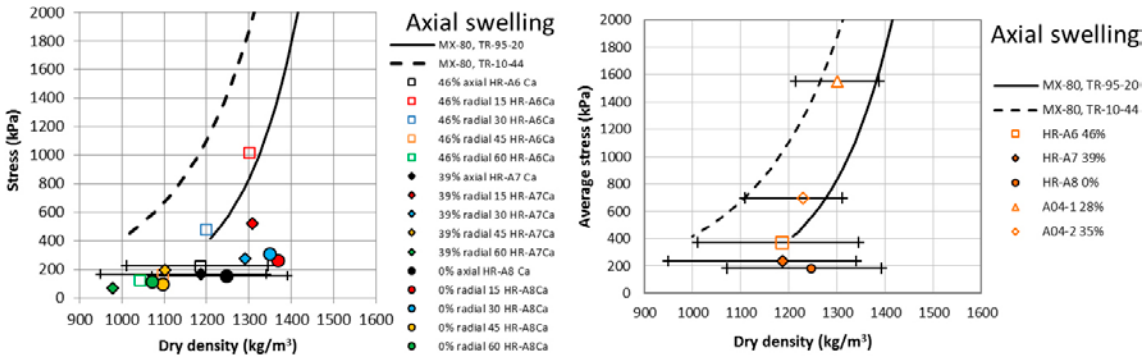

Figure 4-11. *Measured stress as a function of dry density from specimens HR-A6, HR-A7 and HR-A8 (to the left). Calculated average stresses from these specimens and comparable specimens of Calcigel (to the right). Open symbols represent tests reported by Dueck et al. (2016). Models of MX-80 presented by Börgesson et al. (1995) and Åkesson et al. (2010) are also shown. The bars show maximum and minimum dry densities of the specimens and thus illustrate the remaining inhomogeneity.*

Radial outward swelling

The completed test HR-Ro3 with radial outward swelling is presented in Table 4-3. The sampling was done according to Figure 4-3. In Figure 4-12, Figure 4-13 and Figure 4-14 the distributions of water content w, dry density ρ_d and degree of saturation S_r, respectively, at different distances from the bottom and measured after completed test are shown. The evolution of the stresses measured during the test are shown in Figure 4-15 and the results from the last time period, when water pressure was applied, is shown in Figure 4-16. In order to investigate the influence of water pressure 100 kPa was applied on HR-Ro3 for a couple of weeks. In Figure 4-17 the axially and radially measured stresses of HR-Ro3 are plotted as a function of dry density to the left. To the right the corresponding average stresses of HR-Ro3 are shown together with comparable results from previously reported results from this project, i.e. results from HR-Ro1, HR-Ro2, R14-1 and R14-2 where the colours (blue, brown) denote the materials (MX-80, Calcigel).

Table 4-3. Specimens used in the series with radial outward swelling, HR-Ro. The swelling (%) was calculated according to Equation 4-2.

Test ID	Material	Initial water content %	Initial dry density kg/m³	Initial degree of saturation	Constant height mm	Initial diameter mm	Final diameter mm	Swelling %
HR-Ro3	Calcigel	22.6	1 694[1]	103	80	80	96.8	45

[1] Trimmed from larger block with the actual dry density.

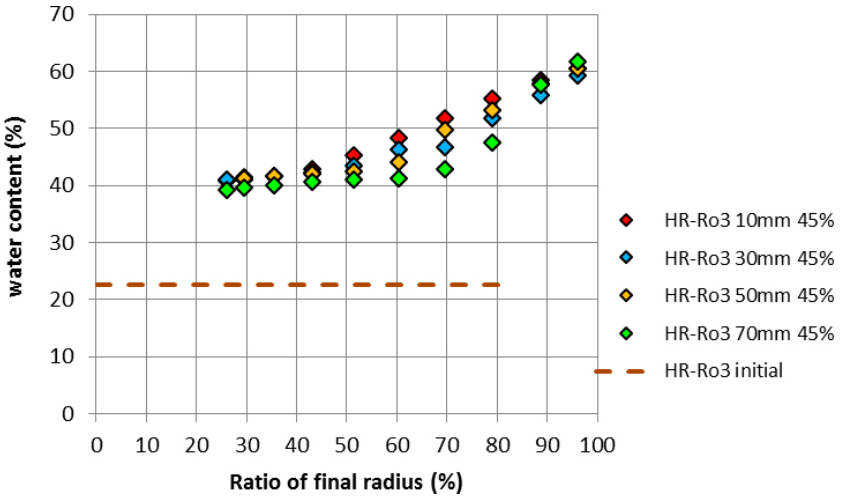

Figure 4-12. *Distribution of water content over the radius of specimen HR-Ro3.*

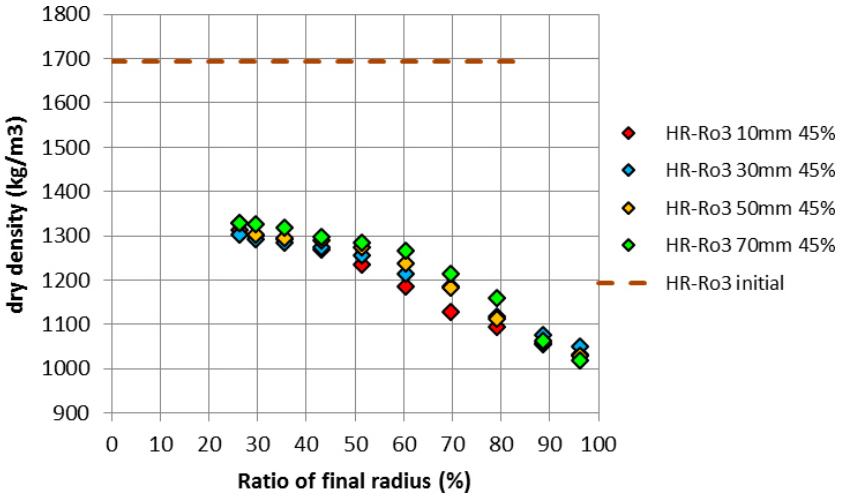

Figure 4-13. *Distribution of dry density over the radius of specimen HR-Ro3.*

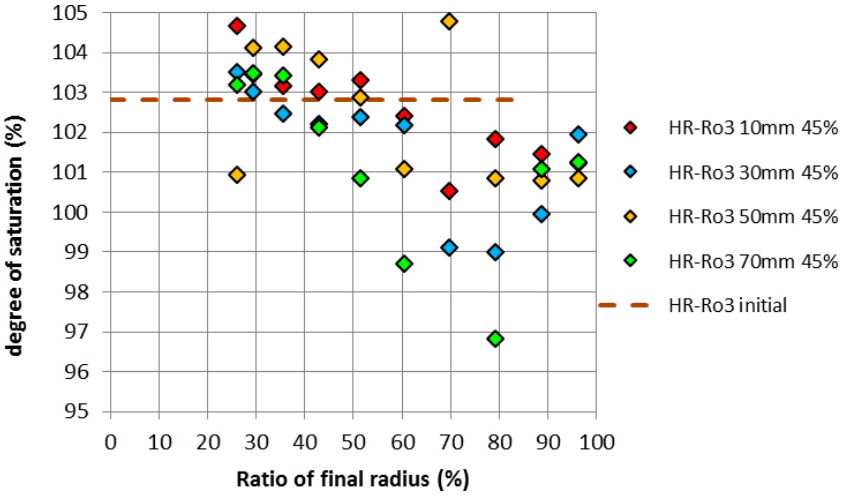

Figure 4-14. *Distribution of degree of saturation over the radius of specimen HR-Ro3, calculated with* ρ_s *= 2 695 kg/m*^{3}*, see also the section with Comments.*

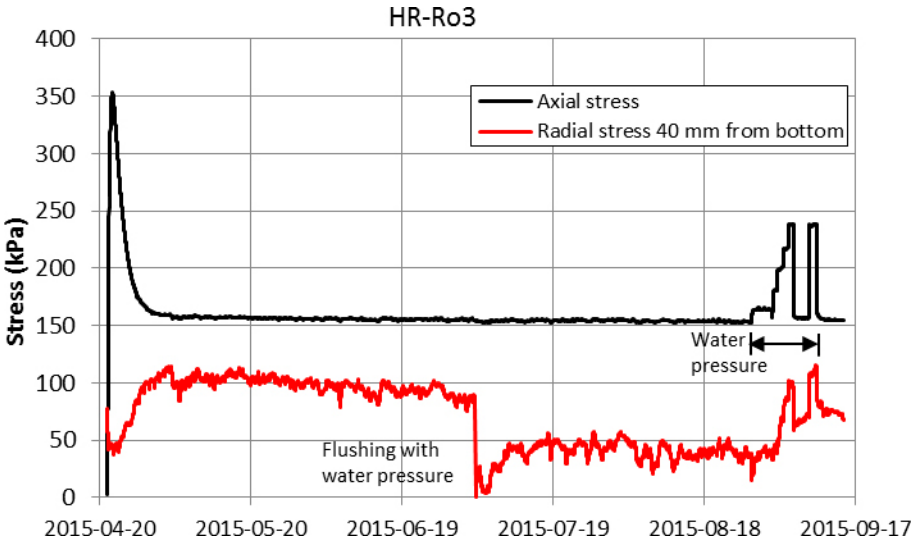

Figure 4-15. *Evolution of total stress with time from specimen HR-Ro3.*

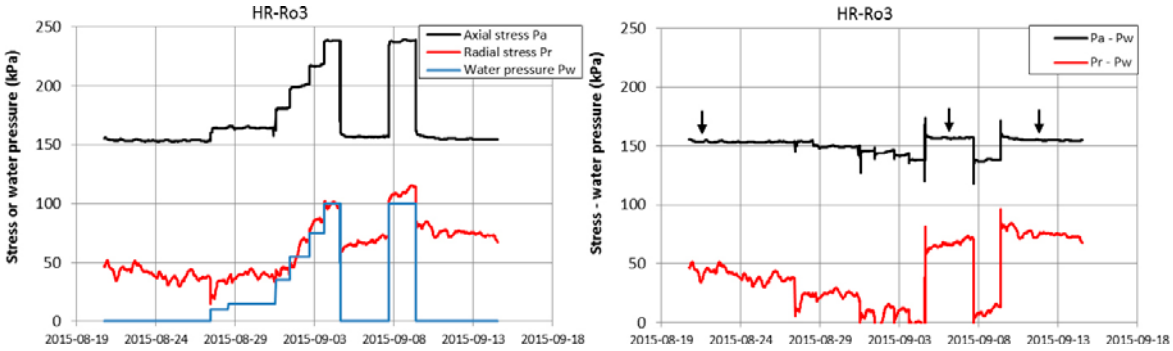

Figure 4-16. *Stress and pressure as a function of time from the last month of HR-Ro3. The measured stresses plotted with the applied water pressure (to the left) and the effective stress, calculated as total stress minus water pressure (to the right). The arrows mark the stresses measured at zero water pressure.*

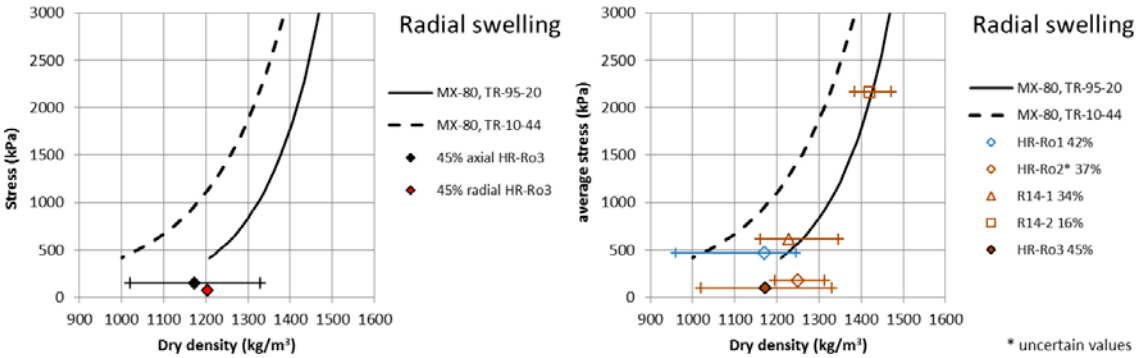

Figure 4-17. *Measured stress as a function of dry density from test HR-Ro3 (to the left). Calculated average stresses from HR-Ro3 and comparable specimens (to the right) where the colours (blue, brown) denote the materials (MX-80, Calcigel) and the open symbols represent tests reported by Dueck et al. (2014, 2016). Models of MX-80 presented by Börgesson et al. (1995) and Åkesson et al. (2010) are also shown. The bars show maximum and minimum dry densities of the specimens and thus illustrate the remaining inhomogeneity.*

Radial inward swelling

The completed test HR-Ri2 with radial inward swelling is presented in Table 4-4. The sampling was done according to Figure 4-3. In Figure 4-18, Figure 4-19 and Figure 4-20 the distributions of water content w, dry density ρ_d and degree of saturation S_r, respectively, at different distances from the bottom and measured after completed test are shown. The evolution of the stresses measured during the test are shown in Figure 4-21 and the results from the last time period, when water pressure was applied, is shown in Figure 4-22. In order to investigate the influence of water pressure 100 kPa was applied on HR-Ri2 for some weeks. In Figure 4-23 the axially and radially measured stresses of HR-Ri2 are plotted as a function of dry density to the left and to the right the corresponding average stresses of HR-Ri2 are shown together with comparable results from previous specimens, i.e. results from HR-Ri1, R21-12, R24-1 and R24-2 where the colours (blue, brown) denote the materials (MX-80, Calcigel).

Table 4-4. Specimen used in the series with radial inward swelling, HR-Ri. The swelling (%) was calculated according to Equation 4-2.

Test ID	Material	Initial water content %	Initial dry density kg/m³	Constant height mm	Outer radius mm	Cavity diameter mm	Swelling %
HR-Ri2	Calcigel	22	1631[1]	80	96.8	48.5	33

[1] Trimmed from lager block with dry density of 1691 kg/m³ with the diameter 95.5 mm.

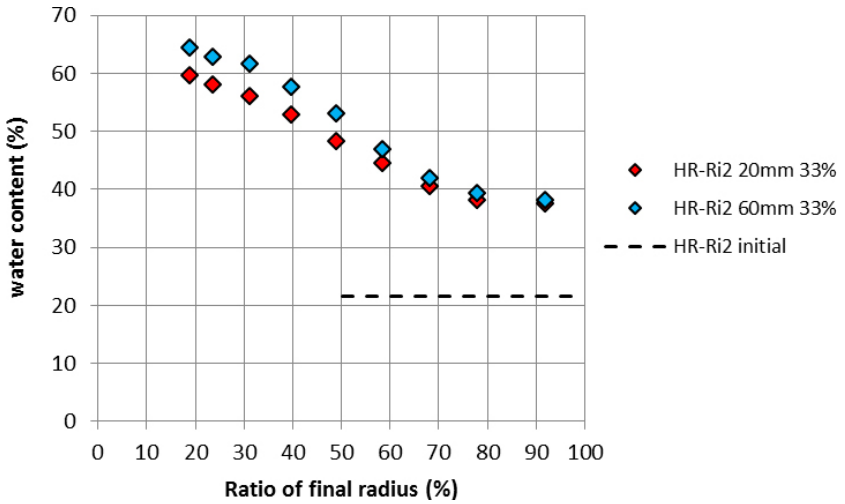

Figure 4-18. *Distribution of water content over the radius of specimen HR-Ri2.*

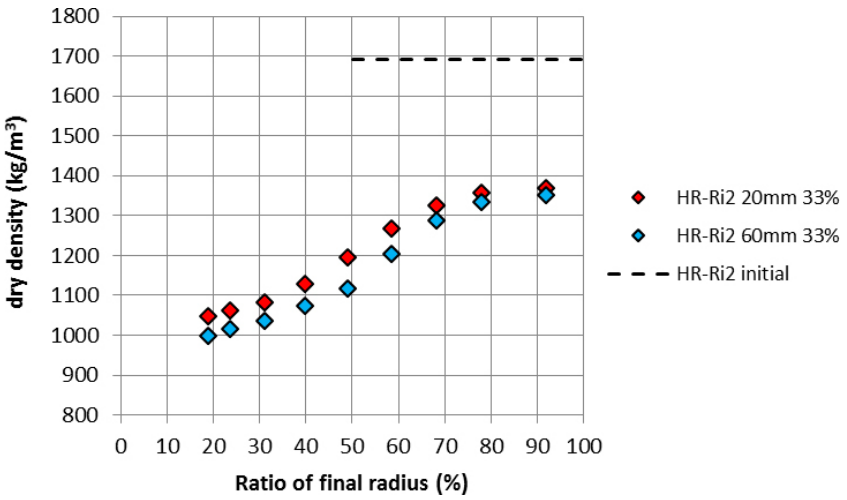

Figure 4-19. *Distribution of dry density over the radius of specimen HR-Ri2*

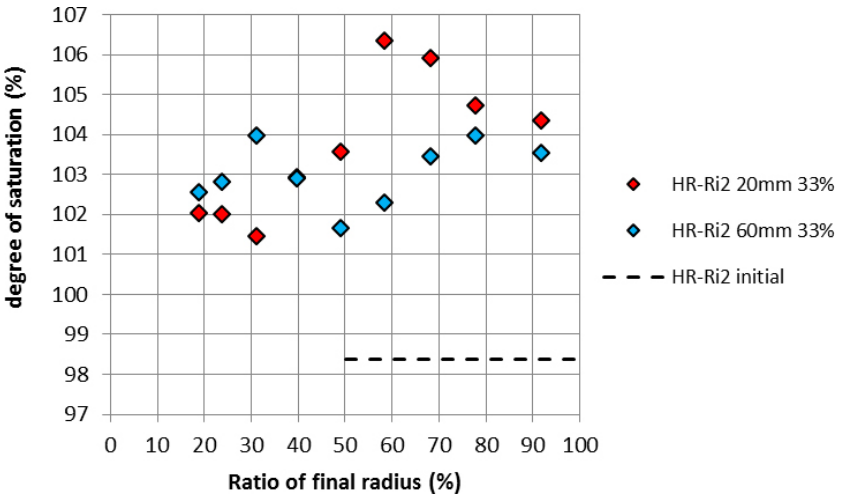

Figure 4-20. *Distribution of degree of saturation over the radius of specimen HR-Ri2, calculated with* ρ_s *= 2 695 kg/m³, see also the section with Comments.*

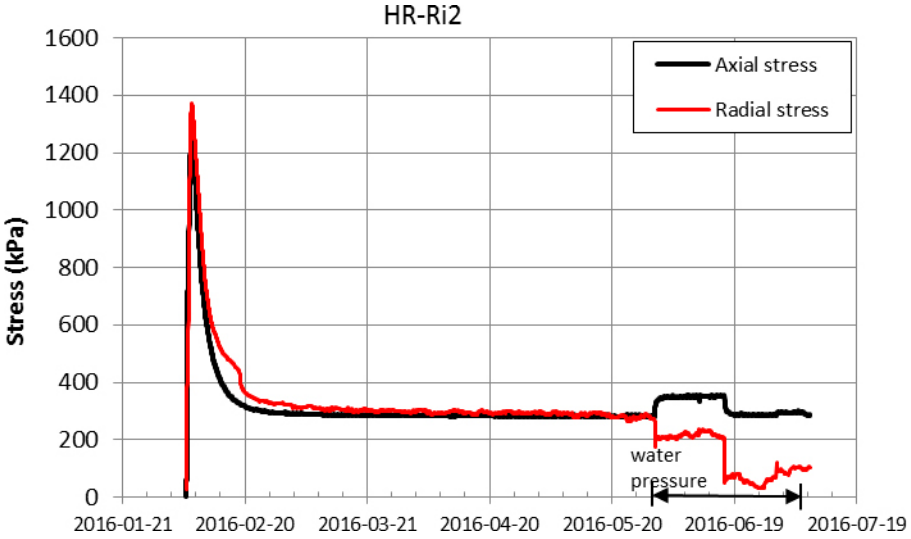

Figure 4-21. *Evolution of total stress with time from HR-Ri2.*

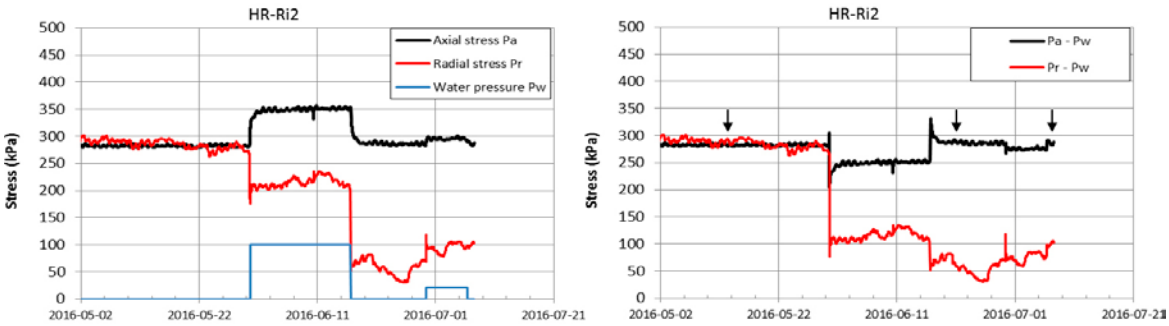

Figure 4-22. *Stress and pressure as a function of time from the last two months of HR-Ri2. The measured stresses plotted with the applied water pressure (to the left) and the effective stress, calculated as total stress minus water pressure (to the right). The arrows mark the stresses measured at zero water pressure.*

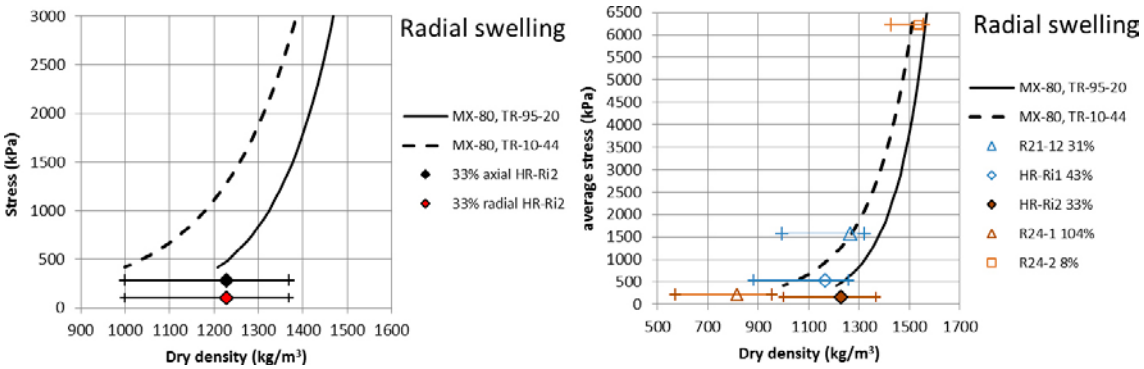

Figure 4-23. *Measured stress as a function of dry density from test HR-Ri2 (to the left). Calculated average stresses from HR-Ri2 and comparable tests (to the right) where the colours (blue, brown) denote the materials (MX-80, Calcigel) and the open symbols represent tests reported by Dueck et al. (2014, 2016). Models of MX-80 presented by Börgesson et al. (1995) and Åkesson et al. (2010) are also shown. The bars show maximum and minimum dry densities of the specimens and thus illustrate the remaining inhomogeneity. Observe the deviating axis comparing to other similar diagrams in this section.*

Comments

In the results from tests on Calcigel in the HR-series the calculated degree of saturation of completed, saturated and dismantled specimens were often above 100 % when based on the particle density ρ_s = 2 695 kg/m^3 (Svensson et al. 2011). If the particle density ρ_s = 2 729 kg/m^3 according to Table 3-1 is used instead the calculated degree of saturation will be lower and the average value of all Calcigel specimens in the HR-A series will be 100 %. In addition, there is a relatively large scatter in the degree of saturation of specimens exposed to radial swelling which probably can be explained by difficulties to get representative samples with the sampling used for these specimens, see Figure 4-3.

Water pressure was applied during the final part of the tests in the HR series presented in this report. Compared to the stresses measured before water pressure was applied the final measured stresses increased or was approximately the same in three of the four tests. In the fourth test, HR-Ri2, the radially measured stress decreased and was lower after than before the water pressure. The reason is not clear but it cannot be excluded that the final part of the measurement, i.e. after the water pressure, is the one that reflects the correct final value of the radial stress.

Tests HR-A6, HR-A7 and HR-A8 were made to compare the homogenisation after swelling 46 % (HR-A6) and 39 %(HR-A7) into an empty space with the homogenisation starting with two specimens having different initial densities and no empty space aiming at the same average density after homogenisation (HR-A8). The final average dry densities of HR-A6, HR-A7 and HR-A8 were 1 185 kg/m^3, 1 186 kg/m^3 and 1 246 kg/m^3 measured after the testing time of 117, 172 and 129 days, respectively. Regarding the measured stresses no large difference was seen between HR-A6 and HR-A7 but the evolution of the measured stresses from HR-A8 was smoother and despite the slightly higher average dry density of specimen HR-A8 the final average stress was less.

The difference in dry density over the height of the specimens was approximately the same in the three specimens but slightly lower in HR-A8, where also the difference in radial stress over the specimen was lower compared to the other two tests. No clear trend of the water pressure used in the final parts of HR-A7 and HR-A8 could be seen.

All test results from the HR-series, except from the isotropic test, are plotted in Figure 4-24 and Figure 4-25 with the average stress as a function of dry density. The bars denote the maximum and minimum stresses and densities and thus illustrate the remaining inhomogeneity. The colours (blue, brown) denote the materials (MX-80, Calcigel) and the symbols (open, solid) denote where the test was presented (previous reports, this report).

It should be noted that HR-Ro3 was run to replace HR-Ro2 since the water supply might have been insufficient to specimen HR-Ro2 which gave uncertain results (marked in Figure 4-17 and Figure 4-25).

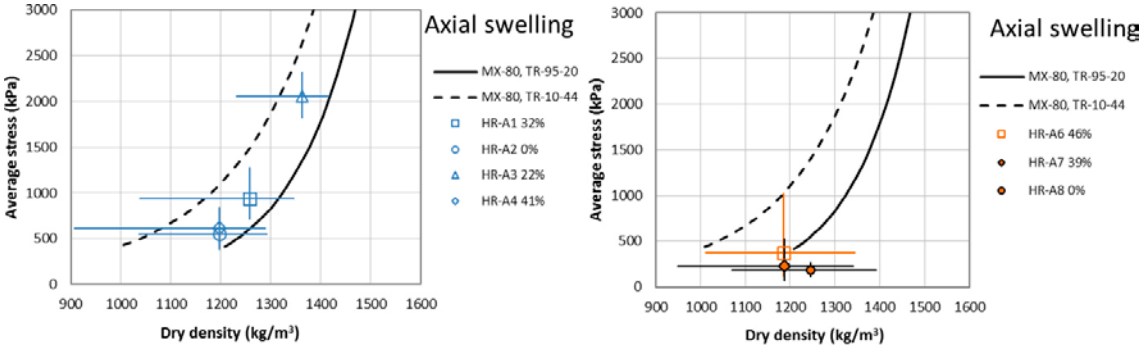

Figure 4-24. *The specimens HR-A1 to A4 (to the left) and HR-A6 to A8 (to the right) are presented as average stress as a function of dry density. The colours (blue, brown) denote the materials (MX-80, Calcigel) and the open symbols denote that the tests were presented by Dueck et al. (2014, 2016). The bars show maximum and minimum dry densities and stresses of the specimens and thus illustrate the remaining inhomogeneity.*

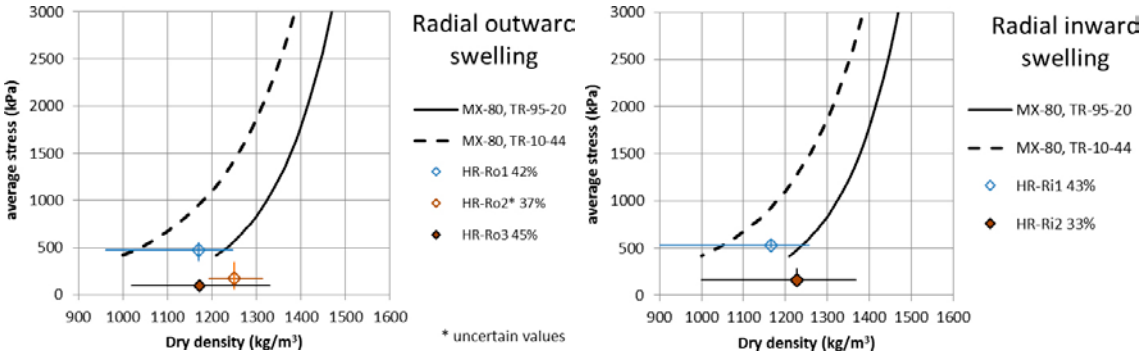

Figure 4-25. *The specimens HR-Ro1 to Ro3 (to the left) and HR-Ri1 to Ri2 (to the right) are presented as average stress as a function of dry density. The colours (blue, brown) denote the materials (MX-80, Calcigel) and the open symbols denote that the tests were presented by Dueck et al. (2014, 2016). The bars show maximum and minimum dry densities and stresses of the specimens and thus illustrate the remaining inhomogeneity.*

4.3 Measurements of friction between bentonite and different surfaces

A series with tests on measurements of friction (Fr) between bentonite and different surfaces has been run. In this section the results from the one not earlier reported is given and additional results from this test can be found in Appendix 2.

Test description

A series with measurements of friction (Fr) between confined specimens at saturation and different types of surfaces has been studied in the project and the majority of the tests have previously been reported. The tests were carried out in the device shown in Figure 4-26. The specimens were saturated with a minimum of swelling and after saturation the friction tests were run where the bentonite was forced through the confining ring having a specially prepared inner surface.

The swelling pressure device consisted of a steel ring surrounding the specimen having filters on both sides. The inner surface of the ring was prepared in different ways; plain steel, lubricated steel, triangular grooves, square grooves or plastic inner surface. Cylindrical specimens were prepared by compaction of powder to a prescribed density and with a diameter of 50 mm and a height of 20 mm. The tests consisted of two phases; the water saturation and the shearing phase. The specimens had free access to de-ionized water during both the saturation and the subsequent shearing phase and the tests were done at constant volume conditions.

During the shearing phase the swelling pressure device was placed in a load frame where the ring surrounding the specimen was fixed while the specimen was moved upwards with a constant rate, i.e. the specimen was pushed upwards through the ring. During the shearing phase the required force to keep the ring in place was measured as well as the deformation and swelling pressure. After moving the specimen a distance similar to the height of the specimen the test was finished and the bentonite specimen was dismantled. The distributions of water content and density over the specimen height were then determined.

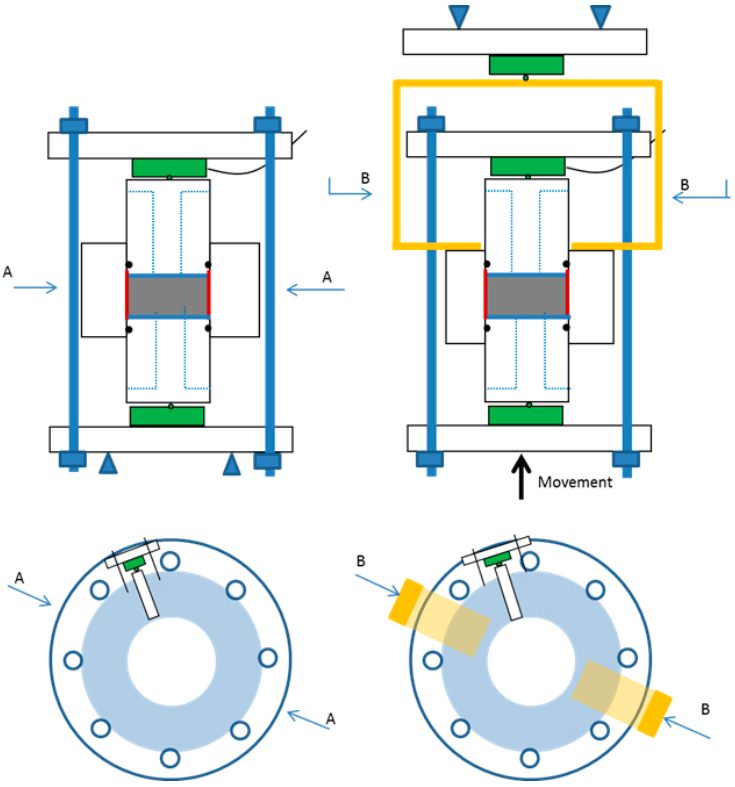

Figure 4-26. *A sketch of the set-up used for the study of friction between the bentonite and different surfaces. The set-up used during saturation (left) and during shearing (right).*

Results (Fr-series)

The friction angle was evaluated from Equation 4-4 where F is the measured force, A_s is the radial surface area of the specimen, P_r is the radial stress perpendicular to the ring, and δ is the friction angle between the ring and the bentonite specimen.

$$F = A_s \times P_r \times \tan(\delta) \qquad \text{(Equaion 4-4)}$$

In Table 4-5 the swelling pressure and evaluated friction angles are presented with average values of w, ρ_d and S_r of the specimen after dismantling. The friction angle was evaluated both as a peak value and a residual value after some deformation and in addition, evaluations based both on the axially measured stress and the radially measured stress were made. The evolution of the swelling pressure with time, measured on top of and under the specimen, is shown in Appendix 2 together with the friction angle evaluated during the entire test evolution.

Table 4-5. Results from measurement of friction between bentonite and a steel surface. The evaluated angle of friction δ is given as a peak value (δ_{peak}) and as a residual value after some deformation at the deformation rate 0.1 mm/min (δ_{res}). Also given are the axially and radially measured stresses before the shearing and the water content, dry density and degree of saturation determined after the tests.

	Measured stress		Friction angle			After dismantling			
	P		δ_{peak}	δ_{res}		w	ρ_d	S_r	
Test ID	kPa	Direction[1]	°	°	Surface	%	kg/m³	%	Type of specimen
Fr2-2	4 333	Radial	8.9	3.7	Grooves (trianglular)	29.2	1 437	90	Compacted Calcigel
	2 968	Axial	12.9	5.3					

[1] Direction of the measured stress.

The results from Fr2-2 is shown together with all comparable results from this test series in Figure 4-27 where the maximum swelling pressure are set to 8 000 kPa and the radially measured stress is used for the evaluation (see also Dueck et al. 2014, 2016). The results are presented with a model of the bentonite friction angel based on triaxial tests presented by Åkesson et al. (2010). In the diagram the colours of the markers denote the feature of the steel surface enclosing the bentonite and the shape of the markers denote the different bentonite materials used.

Comments

Test results in Figure 4-27 (containing all specimens with radially measured stress less than 8 000 kPa from this project, see Dueck et al. (2014, 2016)) show that the peak values in the tests with grooves correspond to the bentonite friction angle and to lower friction angles when other surfaces were used. The difference between the peak and residual values are largest in the tests with grooves and at lower swelling pressure.

The most deviating results, in brackets in Figure 4-27, come from the two tests with pellets, where the swelling pressures are unclear since relatively large difference was seen between stresses measured radially and axially. Since the swelling pressure is unclear and the measured friction forces for these specimens are small the measured friction forces should be further analyzed in the low range of stresses.

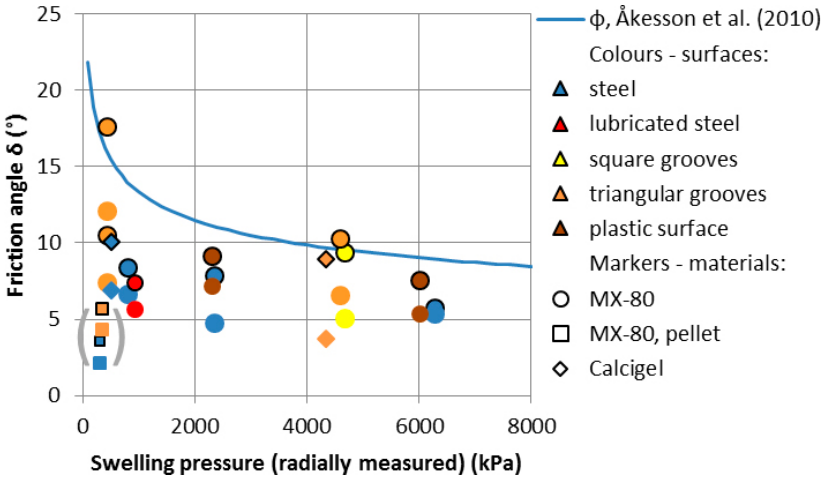

Figure 4-27. *Evaluated friction angles plotted as a function of the radially measured swelling pressure. The colours denote the features of the inner surface of the enclosing ring and the shapes of the markers denote the different materials. The results from the only new specimen Fr2-2 is plotted with the results from all previous comparable specimens with swelling pressure below 8 000 kPa in this project (Dueck et al. 2014, 2016). The results from tests on MX-80 pellet are put in brackets due to uncertainties in the measured swelling pressure. Both peak values (with marker lines) and residual values (without marker lines) are shown.*

4.4 Wetting tests

The series with Wetting tests (W) was made to study the influence of the location of the water supply on the final distribution of dry density. In this section the three tests made in this series are presented. Additional results not shown below can be found in Appendix 3.

Test description – equipment

Three tests were carried out in a set-up shown in Figure 4-28. The specimen consisting of two parts was surrounded by a steel ring. Only one filter for water supply was used and this was placed under the specimen. The top and bottom plates were fixed to the ring in order to keep the volume of the specimen constant. Load cells were placed both on top and under the specimen, each between the fixed plate and a movable piston, where the small deformation required by the load cells was admitted. In some of the tests a load cell was also placed radially, as in the HR-tests. The forces were measured continuously and the transducers were calibrated before and checked after each test.

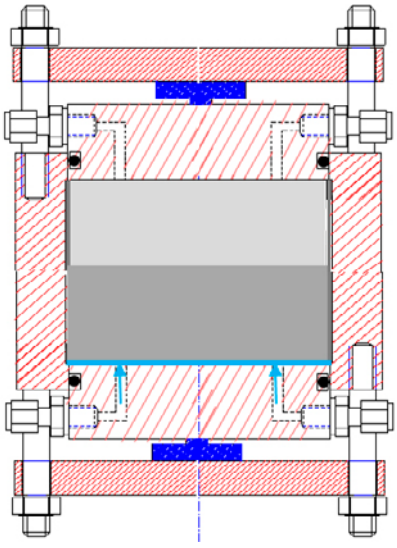

Figure 4-28. *Set-up used for the wetting tests (W) where the specimens consisted of an upper and a lower part with different density. The light blue shows the water supply of the specimens.*

Preparation of specimens

The material used was Calcigel and in each test one part consisted of a compacted sample with high density and a powder sample with low density. The total height of the specimens, including both parts, were 40 mm and the diameter 50 mm.

Test procedure and test series

The specimens with different densities were installed to fill the volume of the test device, i.e. the swelling was minimized. The water supply was made by a continuous circulation of 25 mM $CaCl_2$. After 1–2 months the tests were finished and the distribution of water content and dry density over the specimens were determined. Three tests were run according to Table 4-6.

Table 4-6. Description and test conditions of the lower and upper parts of the three wetting tests. Information is given about how the swelling pressures are measured, i.e. in which direction the stresses are measured, and whether water pressure was used in the tests.

Test ID	Lower part		Upper part		Swelling pressure[1]		Water pressure
	Specimen	Water supply	Specimen	Water supply	Axially measured	Radially measured	Applied
W1-2	Compacted	25 mM $CaCl_2$	Powder	No	Upper and lower	No	No
W1-3	Powder	25 mM $CaCl_2$	Compacted	No	Upper and lower	Mid-height	No
W1-4	Compacted	25 mM $CaCl_2$	Powder	No	Upper and lower	Mid-height	From below

[1] Measured as axial or radial stress.

Results (W-series)

Three wetting tests were run and the initial conditions are given in Table 4-7. The distributions of water content and dry density are shown in Figure 4-29 and Figure 4-30 and the measured stresses are shown in Figure 4-31. In the diagrams the colours (yellow, blue, green) denote the different specimens (W1-2, W1-3, W1-4). Water pressure was used in the test of specimen W1-4 which lasted one month longer than the other tests. The resulting stresses measured during the last month are shown in Figure 4-32.

Table 4-7. Initial conditions of the three wetting tests. The material used was Calcigel.

	Lower part					Upper part				
Test ID	Specimen	H mm	D mm	w %	Dry density kg/m^3	Specimen	H mm	D mm	w %	Dry density kg/m^3
W1-2	Compacted	20	50	12.2	1 550	Powder	20	50	12.2	876
W1-3	Powder	20	50	12.2	876	Compacted	20	50	12.2	1 550
W1-4	Compacted	20	50	11.8	1 550	Powder	20	50	11.8	877

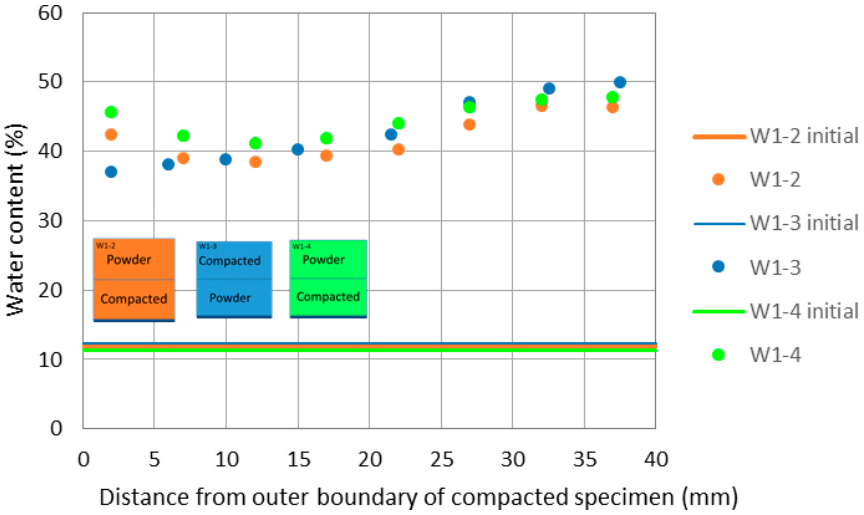

Figure 4-29. *The initial and final water contents shown as a function of the distance from the axial outer boundary of the compacted specimens. The colours denote the different specimens (W1-2, W1-3, W1-4).*

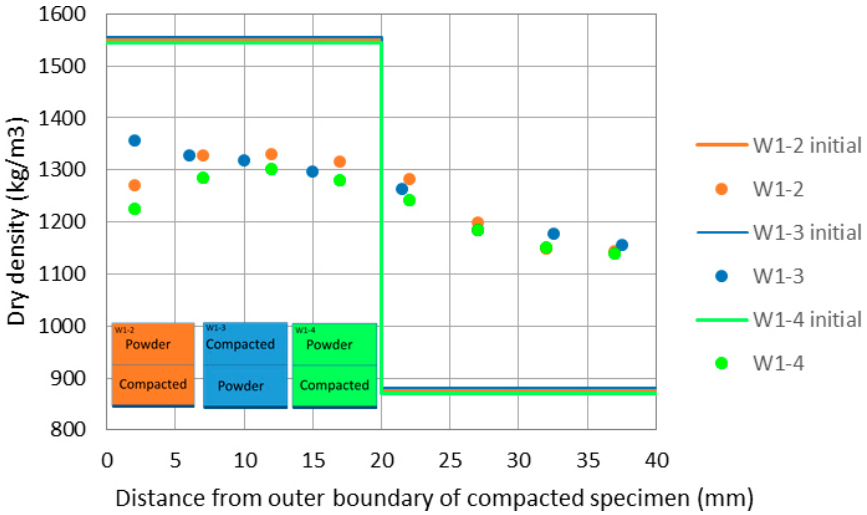

Figure 4-30. *The initial and final dry density shown as a function of the distance from the axial outer boundary of the compacted specimens. The colours denote the different specimens (W1-2, W1-3, W1-4).*

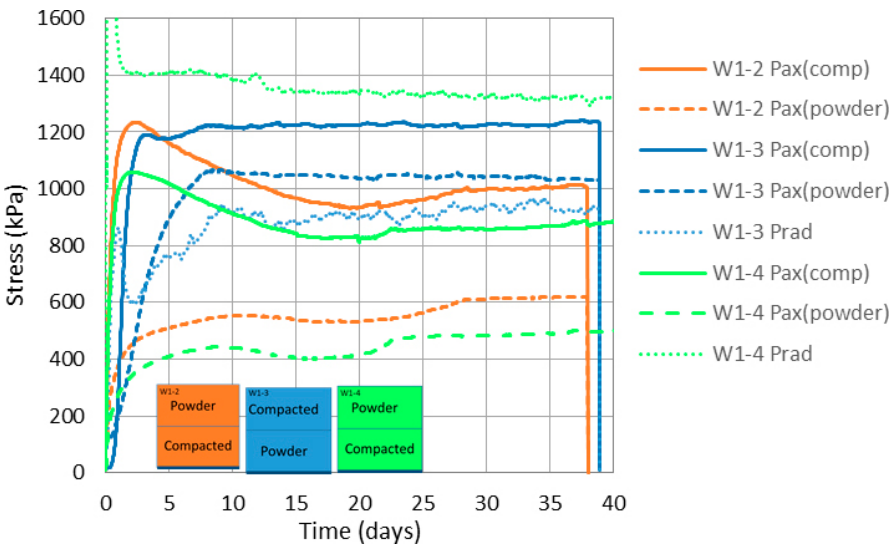

Figure 4-31. *The measured swelling pressure from all three wetting tests are shown as a function of time. The colours (yellow, blue, green) denote the different specimens (W1-2, W1-3, W1-4).*

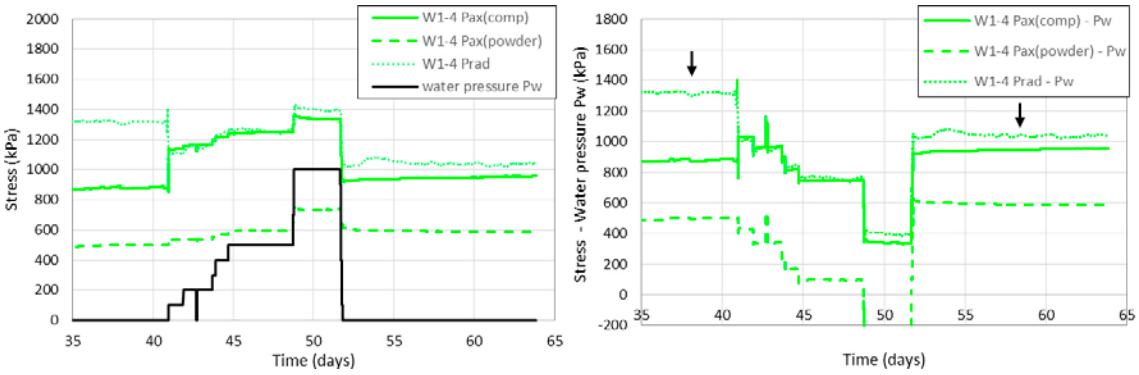

Figure 4-32. *Stress and pressure as a function of time from the last month of W1-4. The measured stresses plotted with the applied water pressure (to the left) and the effective stress, calculated as total stress minus water pressure, (to the right) where the arrows mark the stresses measured at zero water pressure.*

Comments

The swelling pressure measured in the test of the specimen W1-3 (Figure 4-31), where the water was supplied from the powder side, was higher than the swelling pressure of the other two tests. The repeatability, evaluated from the two similar specimens W1-2 and W1-4, was good.

Regarding the distribution of dry density an initial fast swelling and upwards displacement of the compacted sample took place when the water was supplied from this actual side of the specimen, W1-2 and W1-4. The effect of swelling is even larger in the specimen influenced by water pressure, i.e. the homogenisation of W1-4 is somewhat better than of that of W1-2.

Regarding the stresses measured in the test on specimen W1-4 the water pressure seems to have adjusted the radially measured stress from a value higher than both the axially measured stresses to the same value measured axially at the compacted specimen side. It can be noted that the same effect was seen at the use of water pressure applied to HR-Ri2, Figure 4-22. It can also be seen that the axially measured stresses do not fully correspond to the changes in applied water pressure, not even at the final decrease from 1 000 kPa to zero where the decrease of the axially measured stresses were approximately 400 kPa and 150 kPa, respectively.

In Figure 4-33 the difference between the two axially measured stresses from the tests are shown. The difference, which reflects the friction between the specimens and the ring, follows the same trend for all three specimens having an initial peak and then reaching a residual value. The residual values from the two specimens wetted from the side of the compacted sample were 400 kPa while the specimen wetted from the side of the powder was half of that value, i.e 200 kPa.

An interpretation of the evolution of the homogenisation in the three tests can be as follows: When water is available only at the high density side the high density specimen starts to swell from below which results in an upwards displacement of the specimen since no friction against the ring has yet been achieved and the powder has low resistance to compression. With time the swelling pressure from the high density part will cause a strong friction against the ring, which prevents further swelling. This initial displacement, which is seen as a reduced density in Figure 4-30, may move the high density part past the radial transducer and may thus be the reason for the higher radial stress in test W1-4. This initial swelling and high radial stress could also be the reason for the larger difference in axial stress in the two tests W1-2 and W1-4 since it means a stronger friction against the ring.

In Figure 4-34 the results from the wetting tests are plotted as stresses as a function of dry density with horizontal bars showing the maximum and minimum dry density and vertical bars showing the axial stress measured above and below the specimens.

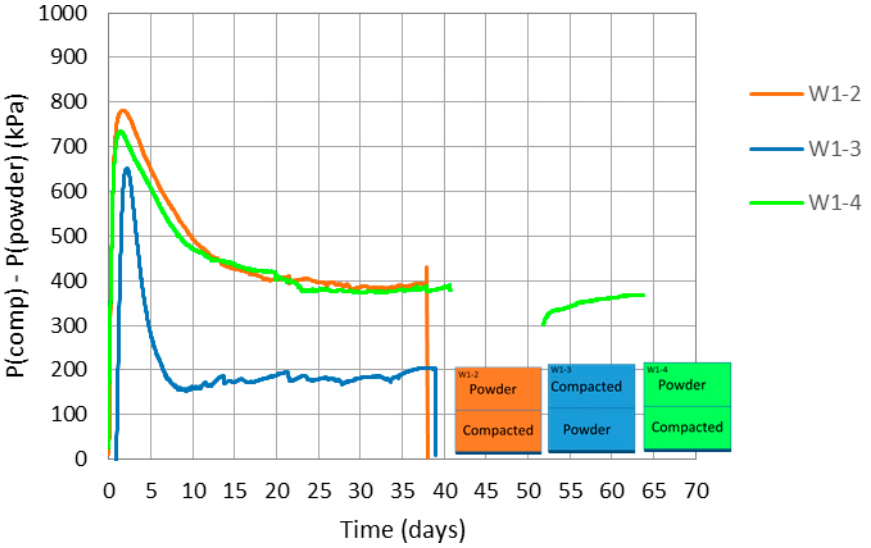

Figure 4-33. *The difference between the axially measured stresses, P(comp)–P(powder), from all three tests.*

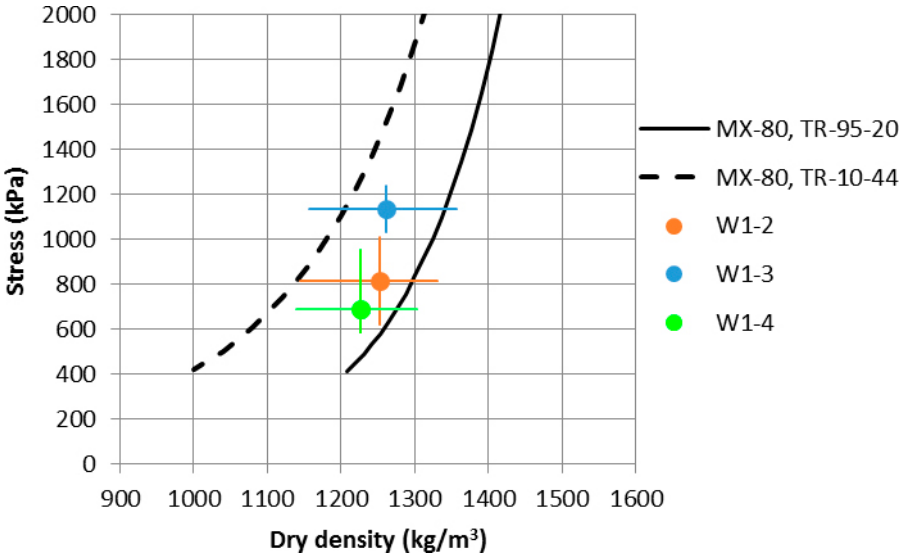

Figure 4-34. *Stress as a function of dry density measured on specimen W1-2, W1-3 and W1-4. The bars show maximum and minimum dry density and the stresses measured above and below the specimens and thus illustrate the remaining inhomogeneity. The results are shown with models of MX-80 presented by Börgesson et al. (1995) and Åkesson et al. (2010).*

5 Homogenisation after loss of bentonite – the self-healing tests

5.1 General

Buffer homogenisation involving loss of bentonite has been studied by two medium scale laboratory tests, called the self-healing tests (SH). The two tests, SH1 and SH2, having the same boundary conditions, started in December 2012. The non-instrumented SH2 was finished and dismantled in May 2014 and the instrumented SH1 was finished and dismantled in September 2015.

The test SH1 should be regarded as the main test of the two, while SH2 was carried through mainly as a trial test where the methods for adding water and for dismantling were tested. The main focus of this section is the detailed description of the test SH1; the preparation, the start condition, the dismantling and the results from the sampling. Important results are also the measured swelling pressure and water potential. SH2 was reported by Dueck et al. (2016).

5.2 Experiment description

The self-sealing ability of large and irregular cavities was studied in this part of the project. Since it was important to be able to determine the final density distribution in detail a suitable combination of block size and cavity size was important to find. The size of the blocks, i.e. cylinder rings, was chosen to be as large as possible, still having a reasonable estimated time to saturation and homogenisation while the size of the cavities was chosen large enough to get good resolution of the sampling after termination of the tests. In addition, the evolution of swelling pressure was measured at strategic points in SH1 in order to follow the evolution of the homogenisation.

Test set-up

The geometry of the set-up used for SH1 is shown with photos in Figure 5-1 and a sketch in Figure 5-2. The positions of the sensors used in SH1 are shown in Figure 5-3. The containment is a very stiff cylinder with the inner diameter 300 mm and the height 100 mm. An inner cylinder with the outer diameter 100 mm is included in the center mainly with the purpose to measure the swelling pressure and RH inside the bentonite block and to reduce the time for saturation and homogenisation. A stiff filter is mounted to the inside of the outer ring with the purpose to provide water to the bentonite from the radial surface. In each bentonite block two cavities were cut out in two diametrical positions in order to simulate loss of material. In the set-up of SH1 nine transducers for measuring swelling pressure and two for measuring suction were included.

Figure 5-2 also shows the geometry of SH2. In addition to the instrumentation, the main differences between SH1 and SH2 were the total time used for the tests (double time was used for SH1 compared to SH2) and the initial size of the cavities (larger cavities were cut in SH2).

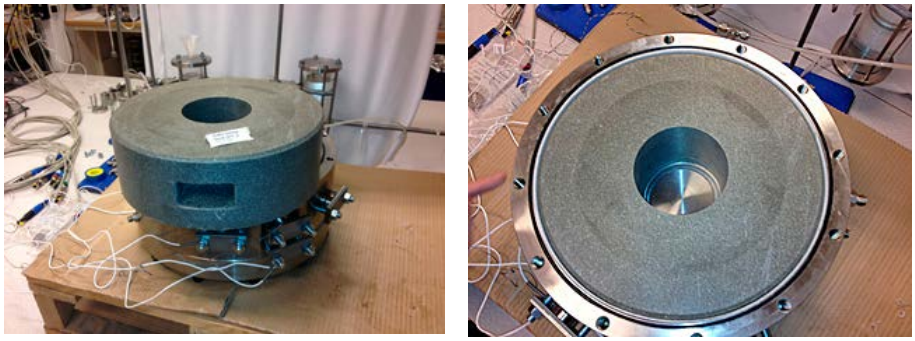

Figure 5-1. *Photos of the device and bentonite block used for SH1. See also Appendix 4.*

Test procedure

The preparation of the bentonite rings for SH1 and SH2 was made by compaction of blocks, which were machined to rings with the correct dimensions and by cutting the cavities. After mounting of transducers, bentonite rings and lids each test was started by filling the filter and the cavities with de-ionized water and applying a low water pressure (10 kPa). The water was supplied through the filters, which were attached to the inside of the cylinder rings. Circulation of water through the filters was possible by use of the water inlet and outlet, located in two diametrical positions of the steel rings, see Figure 5-2.

After about three weeks a steady water pressure of 100 kPa was applied to SH1 and after approximately 11 months 100 kPa was also applied to SH2. During the test period the filters were flushed regularly in order to eliminate air bubbles that may have been collected in the filters.

Both tests were started in December 2012 by the opening of the water supplies to the filters but while SH2 was finished after 17 months (2012-12-17 to 2014-05-13) SH1 was running for 33 months (2012-12-18 to 2015-08-19).

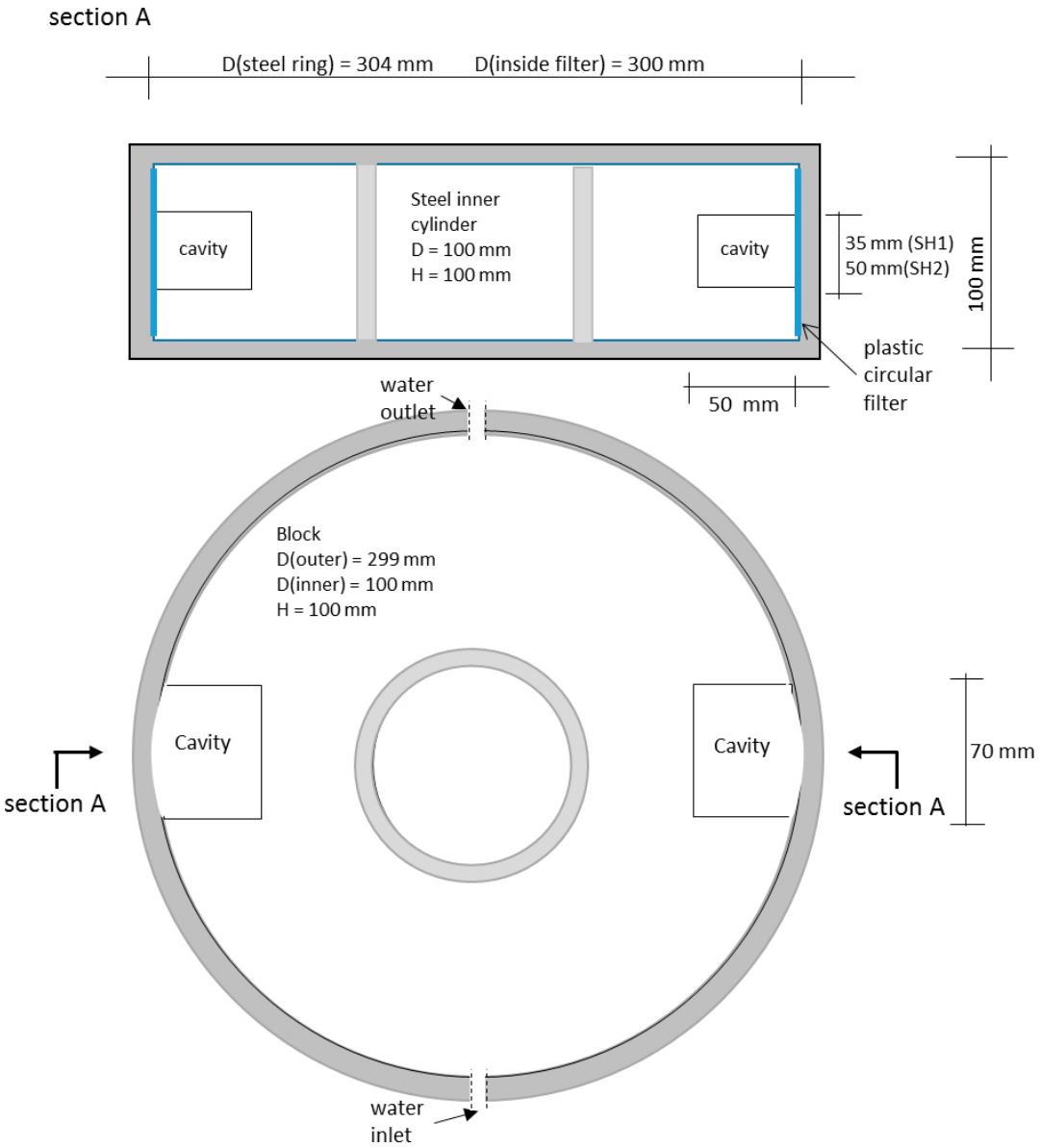

Figure 5-2. *A sketch of the set up used for the tests SH1 and SH2. The dimensions of the outer and inner steel cylinders and the bentonite block with the cavities are shown as well as the plastic filters and the locations of the water inlet and outlet.*

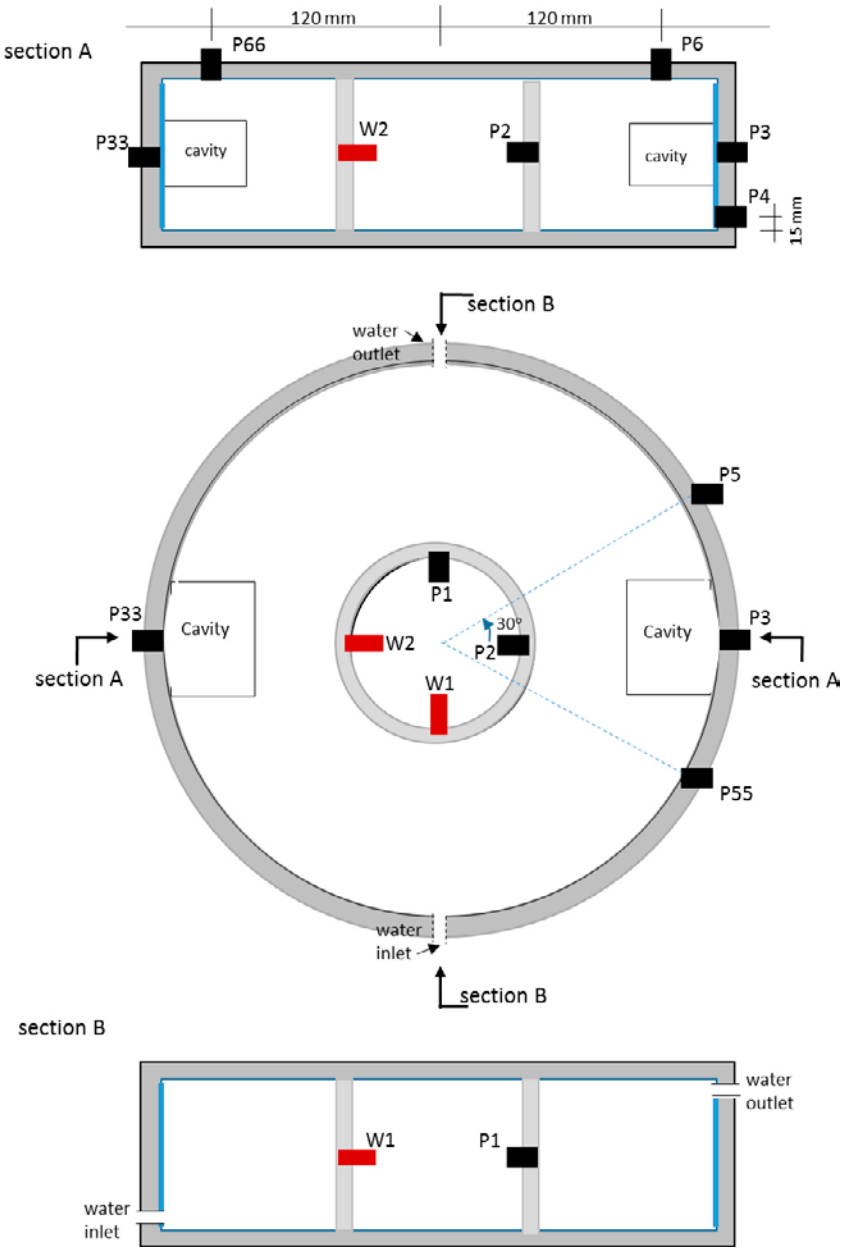

Figure 5-3. *A sketch showing the positions of the sensors used in test SH1. The locations of the cavities and the water inlet and outlet are also shown.*

5.3 Results

The focus of this chapter is the results from SH1. In Appendix 4 additional information about SH1 can be found; additional photos, a timetable for the test and tabulated test results. Results from SH2 were presented by Dueck et al. (2016).

Preparation and installation

The geometry of the test set-up was shown in Figure 5-2. Powder of MX-80 was mixed with de-ionized water to get a water content of 24 % in order to reach a high initial degree of saturation after compaction. Aiming at a dry density of approximately 1 660 kg/m^3 a compaction pressure of 40–60 MPa was used for the uniaxial compacted cylinder block. The block was machined with a rotating lathe to the following dimensions: height = 100 mm, outer diameter = 298.7 mm and inner diameter = 100.0 mm. There was thus a small gap of 0.65 mm between the block and the outer ring and virtually no gap at the inner ring and at the lids. More details from the compaction can be found in Dueck et al. (2016). The density was measured on samples from the removed center

cylinder to 1 657 ± 4 kg/m^3. Cavities were cut in two diametrical positions and the dimensions (height × length × depth) of the cavities in SH1 were 35 × 70 × 50 mm^3, cf. Figure 5-2.

In Table 5-1 the initial condition of the installed bentonite block is presented in terms of bulk density ρ, water content w, dry density ρ_d and degree of saturation S_r. These properties were derived in four different ways (Case 1-4);

1. Initial block density calculated from the initial mass and the initial volume of the block.
2. Initial block density measured on a sample of the removed center cylinder at preparation.
3. Final average density calculated from the initial mass and the final dimensions inside the device without including the cavities.
4. Final average density calculated in the same way as 3 with the filter deformation taken into account without including the cavities.

Table 5-1 Initial conditions of the installed bentonite block in SH1. The base variables bulk density ρ, water content *w*, dry density ρ_d, void ratio *e* and degree of saturation S_r are shown for the initial conditions 1-4.

Case	ρ (kg/m³)	w (%)	ρ_d (kg/m³)	e (–)	S_r (%)	Remarks
1	2029	23.6	1642	0.69	95	Calculated from the initial mass and the initial volume of the block.
2	2047	23.6	1657	0.68	97	Measured on a center sample of the block, sampled at preparation.
3	2009	24.2	1618	0.72	94	Calculated from the initial mass and the final dimensions inside the containment with water in the gap.
4	2006	24.2	1616	0.72		Calculated according to Case 3, with the filter deformation taken into account.

Water saturation and water supply

Water was filled through the inlet pipe and air let out through the outlet pipe (Figure 5-3). The outflow after water fill up was caused by regular water flushing through the filter for de-airing purpose. After one hour approximately 94 % of the available empty space mainly consisting of filter, gaps and cavities, was filled with water. 24 hours after the start approximately 97 % of the available volume was filled. The initial empty space was estimated to 380 ml and the total volume to be filled with water including the saturation of the bentonite was estimated to 470 ml. The water supply was open during the entire course of the test with a constant water pressure of 100 kPa applied after 20 days and then kept constant. The in- and outflow of water for SH1 as a function of time is shown in Figure 5-4.

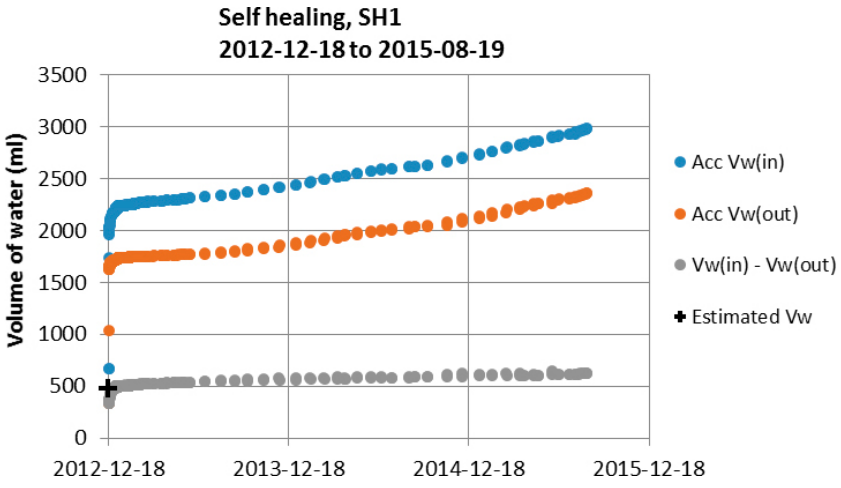

Figure 5-4. *Accumulated in- and outflow of water are shown as a function of time. The netto between the in- and outflow is also shown together with the estimated available empty volume shown with a black plus sign. A water pressure of 100 kPa was applied 20 days after start and then kept during the entire course of the test.*

Swelling pressure and water activity measurements

The results from the swelling pressure measurements in test SH1 are presented in Figure 5-5. The maximum values (blue lines) and minimum values (green lines) were all measured at the outside and at mid-height of the cylinder ring but the minimum values were measured at the center of the cavities and the maximum values were measured well outside the cavities. The locations of the sensors are shown in Figure 5-3. The control of the transducers after the test showed an error less than 2 %.

Measurement of the water potential ψ, Figure 5-6, was made to follow the saturation of the bentonite in positions furthest away from the water source, cf. sensors W1 and W2 in Figure 5-3. The measurements were made by thermocouple psychrometers from Wescor(R) which evaluate the water potential by the Dew Point method (DP) and the Psychrometric method (P). The sensor W1 gave uncertain values from start and stopped working after 7.5 months (from 2013-08-20). The sensor W2 showed decreasing water potential until 16.5 months after start (2014-05-15) and after that no values were measured. After some time though a low constant value was measured with the sensor W2 but at the control after dismantling the sensor did not function properly. However, at the dismantling water was observed inside the casings surrounding the sensors W1 and W2, showing availability of water at the actual positions. This also confirms that the block was completely saturated.

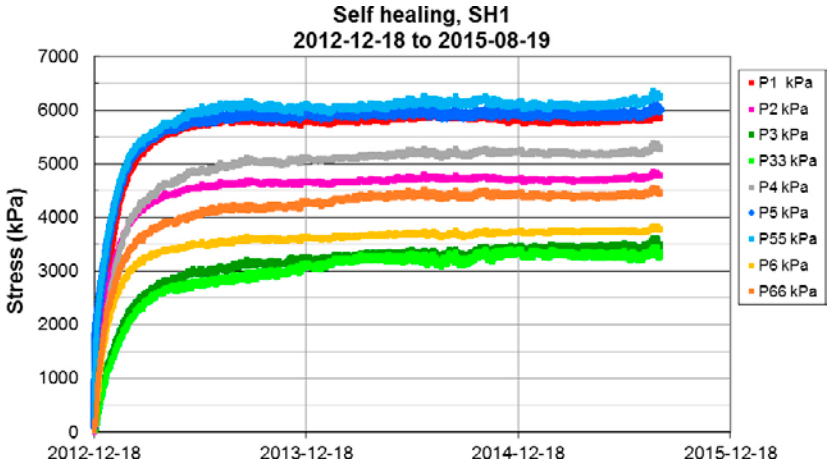

Figure 5-5. *Evolution of swelling pressure from the transducers installed in test SH1. The locations of the sensors are shown in Figure 5-3.*

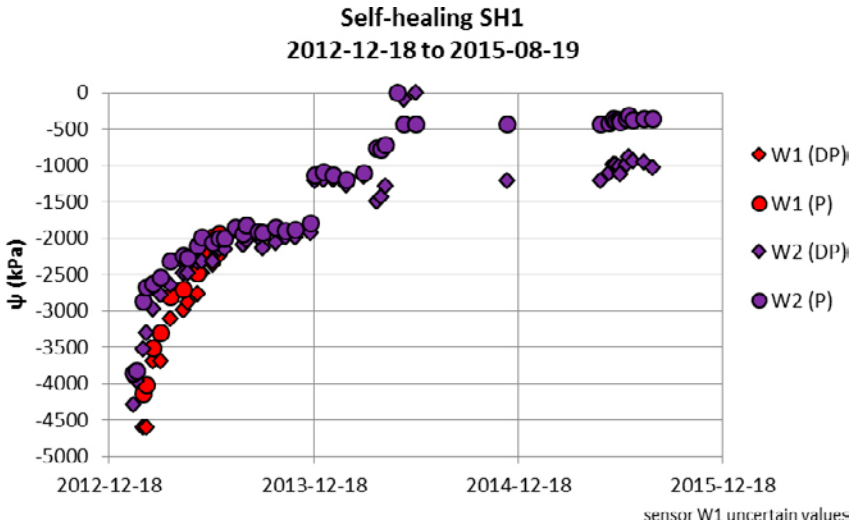

Figure 5-6. *Evolution of water potential (suction) measured with thermocouple psychrometers installed in test SH1. The evaluation was made by both the dew point method (DP) and the psychrometer method (P). The labels show the number of the sensor (W1, W2) and the evaluation method (DP, P). The locations of the sensors are shown in Figure 5-3.*

Termination and dismantling

The test was terminated on 2015-08-19 and five days before the termination the applied water pressure of 100 kPa was lowered to zero. Before the opening of the device an attempt was made to evacuate the filter from water but only a small volume of water was possible to remove. The dismantling started with lifting the lid and removing the bottom from the cylinder ring and then marking the planned sampling on the uncovered bentonite surfaces. The dismantling continued by free-drilling and removing the inner steel cylinder and dividing the bentonite cylinder into two half circles by sawing radially. Figure 5-7 shows photos taken during the dismantling.

Sampling and denomination of the samples

The bentonite cylinder ring was divided into two half-cylinders during the dismantling. One of the half-cylinders was directly used for the sampling and determination of water content and density distributions while the other one was sealed and stored for later analyses. The division of the bentonite ring in different parts and the sampling plan are illustrated in Figure 5-8 and Figure 5-9.

The half-cylinder for sampling was further divided axially at mid-height and the determinations of density were made on the upper part while the determinations of water content were made on the lower part, illustrated to the right in Figure 5-8. Extensive sampling was made with two different strategies, i.e. along four lines and continuously within a sector. The lines and the sector are marked red and yellow, respectively, to the left in Figure 5-8.

The lines were located at the approximate angles 0°, 20°, 65°, 85° and 95° from the middle of the initial cavity and samples taken along these lines were denominated L0, L20, L65, L85 and L95, see Figure 5-9. The sector with continuous sampling was located between 0° and 45° from the middle of the cavity and it included parts both inside and outside of the initial cavity. The sector was divided into the sub-sectors A, B, C and D with the center angles 6°, 17°, 28° and 39°, respectively, from the center of the cavity. The sub-sectors A to D were further divided into two parts each, along which the samples were taken. The denominations of all subsectors starting from the center of the cavity are A(2), A(1), B(2), B(1), C(2), C(1), D(2), D(1), see Figure 5-9. Both the water content and the density were determined at three different levels axially; 1 – outermost, 2 – second outermost and 3 – innermost, which are illustrated to the right in Figure 5-9. The approximate size of each type of sample is shown in Figure 5-10.

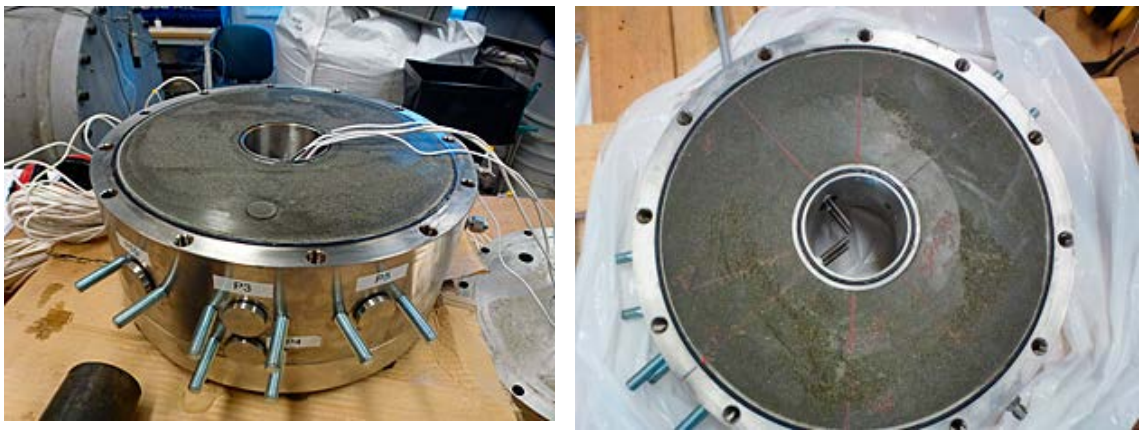

Figure 5-7. *Photos from the dismantling of SH1 just after lifting the lid. See also Appendix 4.*

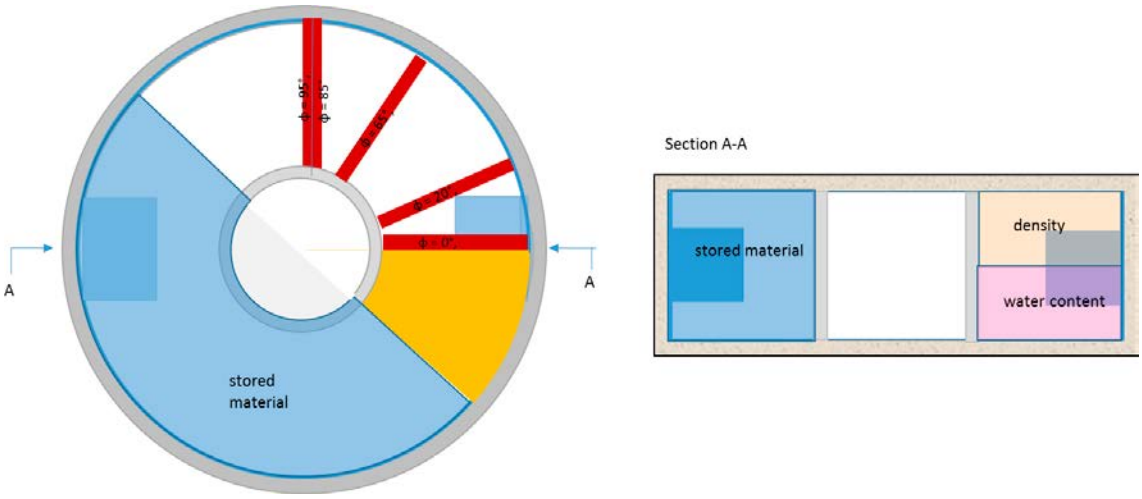

Figure 5-8. *Plan view (to the left) and section (to the right) of the bentonite block at dismantling. The plan view shows the bentonite cylinder ring with the stored material (blue area), the lines of sampling (red lines) and the sector for continuous sampling (yellow area) marked. The section shows the stored part and the parts used for determinations of density and water content.*

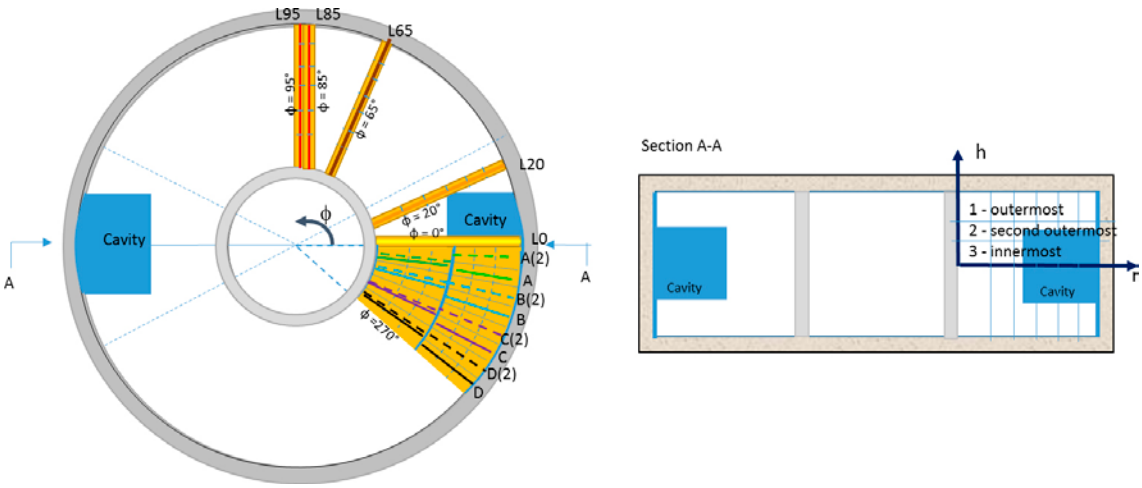

Figure 5-9. *Plan view (to the left) which shows the sampling along lines at different angles from the middle of the cavity; 0° (yellow), 20° (orange), 65° (brown) and 85°/95° (red) and the sampling continuously within a sector along the dotted and solid lines (green, blue, purple and black). The section (to the right) shows the different axial levels for the sampling; outermost, second outermost and innermost.*

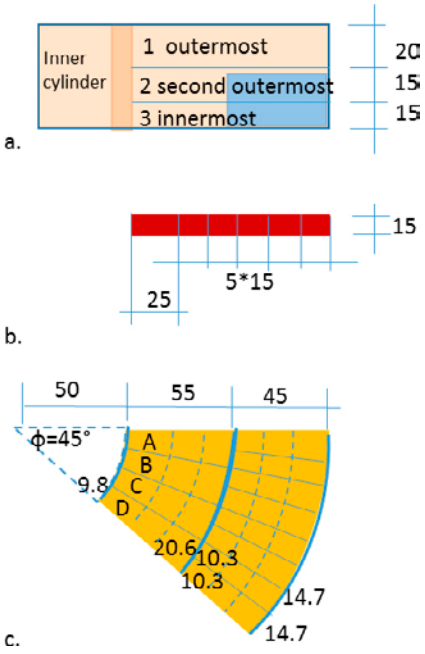

Figure 5-10. *Positions and sizes of the samples. Different parts and views are shown; a. section with different sampling levels, b. plan view of one of the five sampling lines and c. plan view of the sampled sector with subsectors. The numbers show the approximate dimensions of the samples in the unit mm. As shown the center angle of the sampled sector is 45°.*

Distribution of water content and density of SH1

The measured distributions of dry density determined after dismantling of SH1 at the levels 1, 2, and 3 (outermost, second outermost and innermost) are shown in Figure 5-11, Figure 5-12 and Figure 5-13, respectively. The dry densities of the samples from the sector were calculated from the measured bulk densities and water contents. For the samples along the lines the dry densities were calculated from the measured water contents and a degree of saturation of 100 % which was proven to be valid in areas where this was analyzed, see below. In each diagram a small illustration of the location of the samples is given. The initial dry density of the block was approximately 1 657 kg/m^3, see Table 5-1. The average final density based on the initial mass and the final volume of the device, i.e. with the cavities taken into account, was calculated to 1 568 kg/m^3.

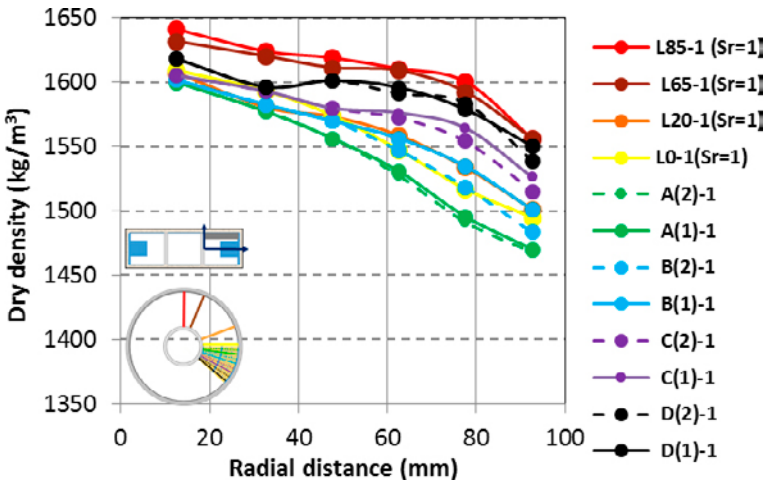

Figure 5-11. *Distribution of dry density at the outermost level 1 in different directions. The colours (red, brown, orange, yellow, green, blue, purple, black) show the angles (85°, 65°, 20°, 0°, −6°, −17°, −28°, −39°) to the center of the cavity. The values are calculated from measured water contents and 100 % water saturation when the labels include (Sr = 1).*

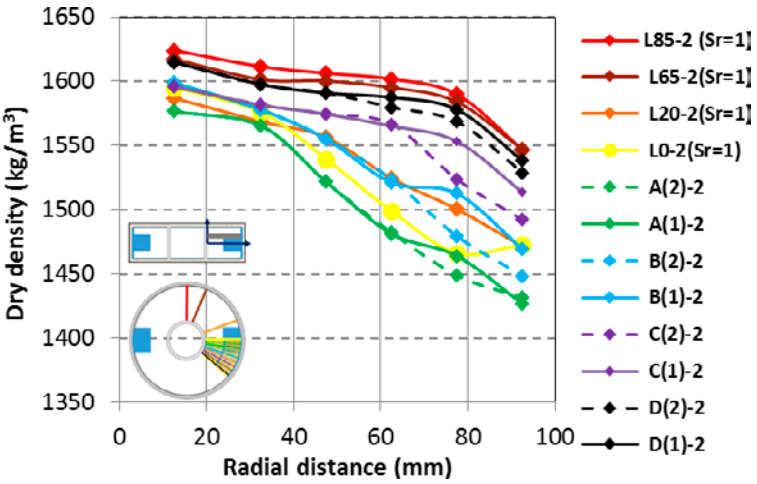

Figure 5-12. *Distribution of dry density at the second outermost level 2 in different directions. The colours (red, brown, orange, yellow, green, blue, purple, black) show the angles (85°, 65°, 20°, 0°, −6°, −17°, −28°, −39°) to the center of the cavity. The values are calculated from measured water contents and 100 % water saturation when the labels include (Sr = 1).*

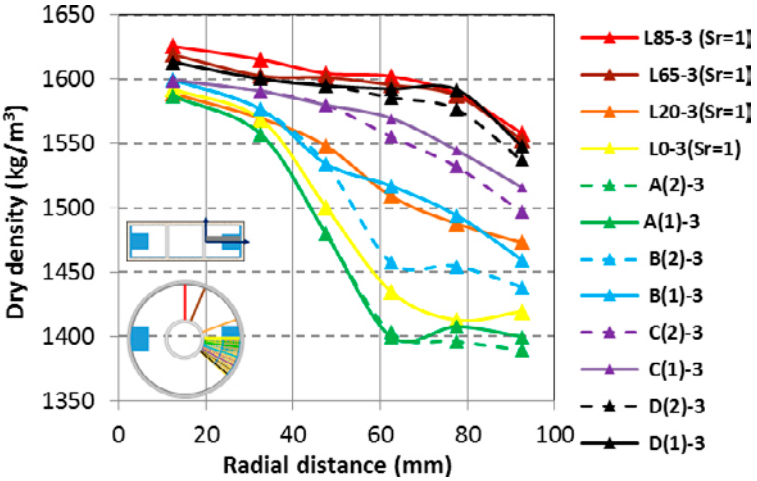

Figure 5-13. *Distribution of dry density at the innermost level 3 in different directions. The colours (red, brown, orange, yellow, green, blue, purple, black) show the angles (85°, 65°, 20°, 0°, −6°, −17°, −28°, −39°) to the center of the cavity. The values are calculated from measured water contents and 100 % water saturation when the labels include (Sr = 1).*

The distribution of dry density in different directions are shown as a function of the radial distance. The colours (red, brown, orange, yellow) show the results from the sampling lines (L85, L65, L20, L0) at the angles (85°, 65°, 20°,0°) from the center of the initial cavity. Within the sector with continuous sampling the colours (green, blue, purple, black) show the sampling lines at the angles (6°, 17°, 28°, 39°) from the center of the initial cavity. Each subsector was further divided into two parts, marked with dotted and solid lines of each of the colours and from the center of the cavity the denomination of all sub-sectors are A(2), A(1), B(2), B(1), C(2), C(1), D(2), D(1).

The lowest values (green points) and the highest values (red points) were seen in the directions coinciding with and perpendicular to the direction of the cavity, respectively. A comparison of densities at the outermost (Figure 5-11), second outermost (Figure 5-12) and innermost (Figure 5-13) levels give generally decreasing densities, which is logical. In Appendix 4.3 tabulated values of the distribution of water content and dry density are given.

Comments

The diagrams show that the dry density increases logically from the lines through the center of the cavity (A(2) and L0, green and yellow lines) to the lines perpendicular to the center of the cavity

(L85/L90, red lines). The relatively low density of the samples at the radial distance of 92 mm, and at all three levels, of the most distant peripheral part L85 (red lines) was probably caused by the 0.65 mm gap between the bentonite ring and the outer ring with filter.

In addition, to the results presented above samples were taken in order to study the vertical symmetry mirrored by the horizontal symmetry plane, i.e. the correspondence between the results from samples taken from the upper and from the lower half of the bentonite ring. Along line L85 the water content was determined at all levels on both the lower half (levels 1, 2 and 3) and the upper half (here called levels 4, 5 and 6). The results are shown in Figure 5-14 where each colour represents a specific level, i.e. outermost, second outermost and innermost. The water contents determined on samples from the upper and lower half agree well and the maximum difference is seen between the outermost samples at the outermost radial distance which differ 0.6 %.

In the results from the sampled lines, i.e. L0 to L85, presented in Figure 5-11 to Figure 5-14 only the measured distribution of water content was taken into account and for the calculation of dry density the degree of saturation was assumed to be 100 %. Within the 45° sector and along one of the sampling lines, the measured bulk densities were also analyzed and the degree of saturation calculated. Within the sampled sector the degree of saturation was analyzed at 108 points and the values varied between 99 % and 102 % with an average of 101 %, Table 5-2. Along the sampling line L85 all samples, from both the upper and lower part of the bentonite ring, were used for determination of water content. In parallel, bulk densities were measured on all samples taken from the sampling line L95, i.e. from both the upper and lower part of the bentonite ring. From the water contents and bulk densities measured along L85 and L95 the degrees of saturation were calculated. In those 36 points along the sampling lines and in addition to the samples referred to in Table 5-2 the degree of saturation varied between 100 % and 103 % with an average of 101 %.

Table 5-2. Degree of saturation of all samples from the 45° sector.

	Degree of saturation %	Number of samples
	99	2
	100	19
	101	59
	102	24
	103	4
	104	
Average	101	
Sum		108

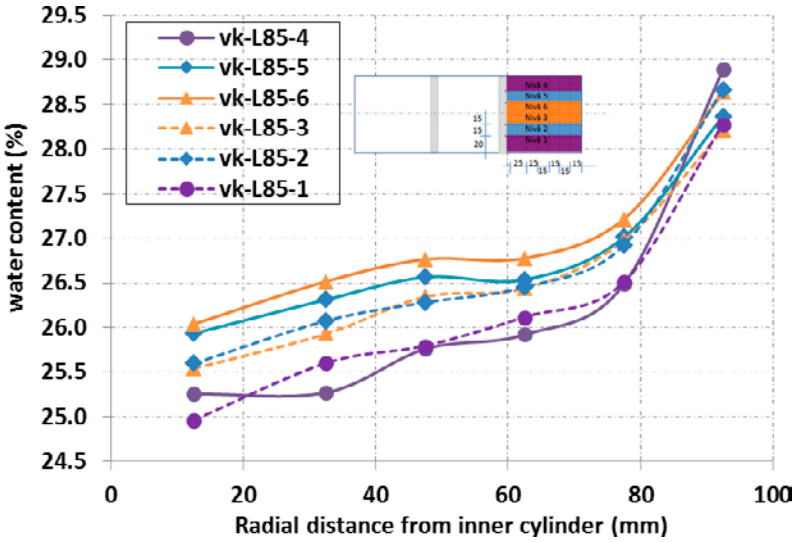

Figure 5-14. *Water contents determined on samples taken along the sampling line L85. Samples were taken from both the upper half (solid lines) and lower half (dotted lines) of the bentonite ring. The colours (purple, blue, orange) show the levels (outermost, second outermost, innermost).*

6 Homogenisation in long tubes

6.1 General

Swelling and homogenisation in long tubes are studied with this test type where ten tubes having similar designs and content are used. The heights of the tubes are 250–350 mm and the diameters are 25–35 mm and while the lower half of each tube is filled with highly compacted bentonite the upper half is filled with bentonite pellets. Water is added from the upper end, i.e. above the pellets. Swelling pressure is determined from some of the tubes by measuring radial and axial stresses exerted on pistons with certain areas. By different test durations of the tubes the distribution of density and the evolution of swelling pressure can both be studied as a function of time. One test was finished after 2 years while nine are still ongoing.

The purpose of this test type is to study:

- the effect of friction for limiting homogenisation,
- the influence of time on the remaining density gradients after completed swelling and compression.

In addition to study the ability of the bentonite to homogenise the result can also be applied to evaluate to what extent the so called “transition zones” in tunnels can be used to downshift the swelling pressure against e.g. a plug.

6.2 Experiment description

Test set-up

A general sketch of the set-up used in this series is shown in Figure 6-1. The height of the tubes is ten times the diameter and the tubes were placed in an upright position during the tests. The lower half of the tubes was filled with highly compacted bentonite and the upper half was filled with bentonite pellets. The material used in this test type was MX-80. The tube wall contained milled grooves to increase the friction between the bentonite and the tube.

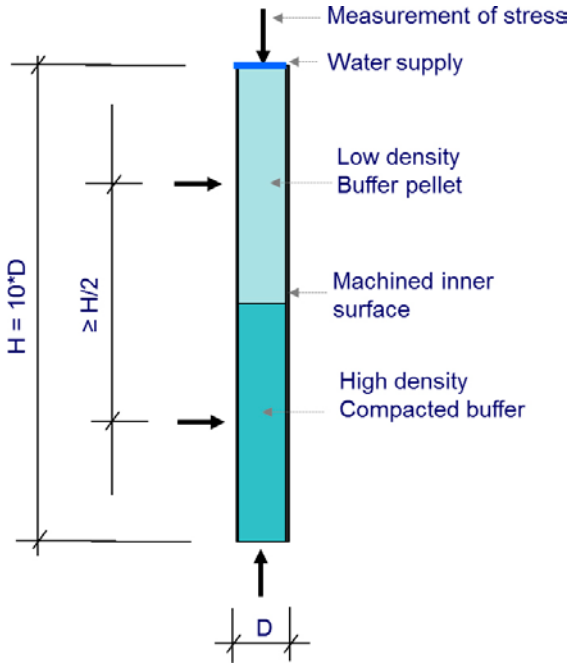

Figure 6-1. *Sketch of the set-up used for the series with long tubes.*

Four different varieties of the tube were manufactured with the main difference being the features of the inner wall and the dimensions of the tubes, Figure 6-2. The features of the inner walls are marked with different outer lines in Figure 6-2; square shaped grooves (grey lines), triangular shaped grooves (black lines) and smooth inner wall (no lines). The different types of grooves are shown with greater details in Figure 6-3 and with the photos in Figure 6-4. Two different dimensions of tubes were used and while nine had the diameter 25 mm (and height 250 mm) one had the diameter 35 mm (and height 350 mm). The specimens FLR1 to FRL4 were run according to Figure 6-2 while specimens FLR5 to FLR10 were run with similar conditions as FLR2 but without any measurements of swelling pressure. Details about specimens FLR1 to FLR10 including the initial dry density are shown in Table 6-1.

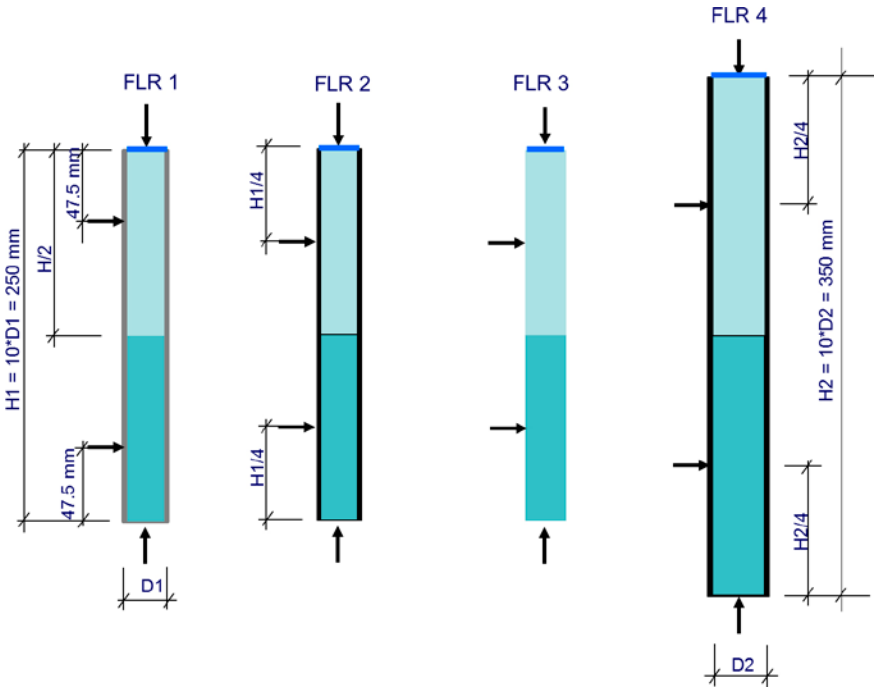

Figure 6-2. *Sketches of the tubes used in the test series and the boundary conditions of the specimens FLR1 to FLR4. The different lines surrounding the specimens (grey line, black line, no line) denote the different features of the inner surface of the tubes (square grooves, triangular grooves, polished smooth). The specimens FLR5 to FLR10 were run in tubes similar to the one used for specimen FLR2 but without swelling pressure measurements.*

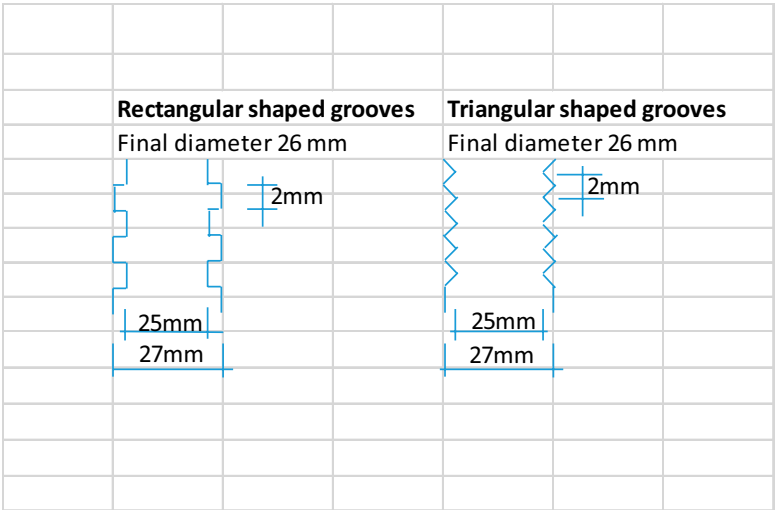

Figure 6-3. *Sketch of the rectangular and triangular shaped grooves inside the tubes.*

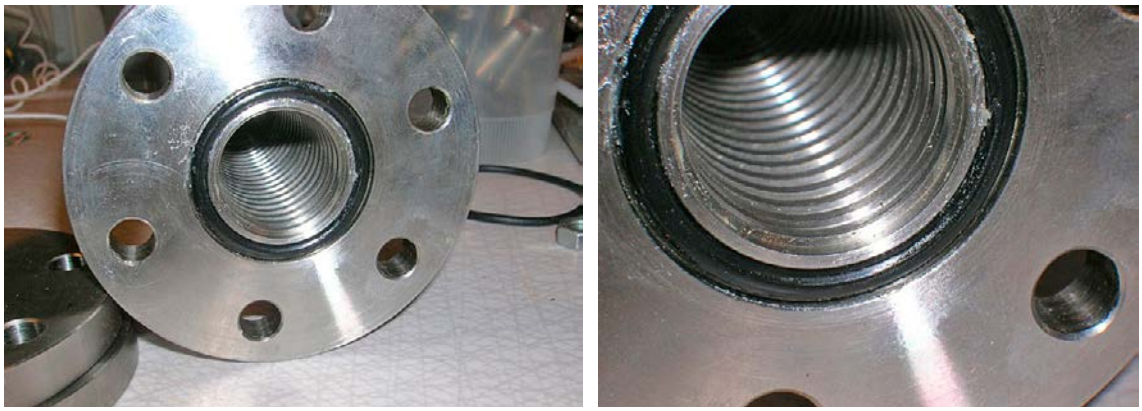

Figure 6-4. Photos of the rectangular shaped grooves inside the tube used for specimen FLR1.

Table 6-1. Test conditions and target initial densities for all specimens in the series with long tubes.

Test ID	FLR1	FLR2	FLR3	FLR4	FLR5	FLR6	FLR7	FLR8	FLR9	FLR10
Set-up										
Total height (mm)	250			350	250					
Final average diameter (mm)	26	26	25	36	26					
Inside friction (grooves)	Rectangular	Triangular	Smooth	Triangular	Triangular	Triangular	Triangular	Triangular	Triangular	Triangular
Transducers	Yes				No					
Material upper half	MX-80 pellet (extruded)									
Material lower half	MX-80 buffer									
Water supply	Only from the pellet side and initially added by circulation									
Type of water	2 mM NaCl									
Target dry density (after swelling)										
Upper part $\rho_{d,upper}$ (kg/m^3)	772	882	882	882	882	882	882	882	882	882
Lower part $\rho_{d,lower}$ (kg/m^3)	1566	1561	1561	1561	1561	1561	1561	1561	1561	1561

Test procedure

The compacted material in the lower part of the tubes was prepared by compression of powder to 5 samples with the height and diameter 25 mm and 24.9 mm, respectively (or in case of FLR4 the height 35 mm and diameter 34.5 mm) which, were placed on top of each other in the tubes. The upper part with pellet was prepared by dividing each pellet into two pieces and putting them in place by hand to achieve the predetermined density. After closing the tubes with pistons in both ends load cells were attached to the instrumented tubes.

The test started by adding a solution of 2 mM NaCl to the upper drainage, see Figure 6-5. The water was initially added by use of vacuum but after the initial phase a peristaltic pump was attached to the system to be used for the regular water circulation. After the planned testing period the tubes are dismantled and the distribution of water content and density are determined with as good resolution as possible.

To be able to study the time effect of the density gradient, different testing periods were planned for the ten tubes. The date of the dismantling of the last tube has not yet been decided but the non-instrumented tubes will be dismantled before the instrumented ones. The first dismantling was done already after 2 years and the second and third dismantling are planned to be made after 4 and 8 years, respectively.

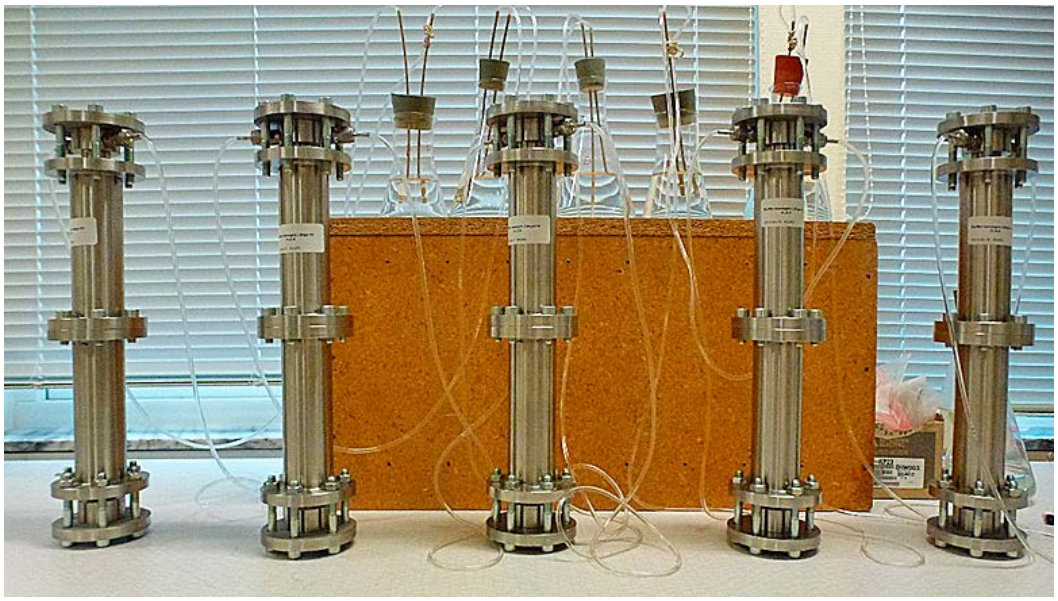

Figure 6-5. *Test tubes used for specimens FLR6 to FLR10 each attached to tubes used for water circulation on a regular basis.*

6.3 Results

The focus of this chapter is the results of the dismantled FLR5. In Appendix 5 additional information is given.

Preparation and installation

The results from the preparation and installation are given in Table 6-2.

Table 6-2. Data from the installation of the 10 tubes in the test series, FLR1 to FLR10. The average degrees of saturation are given before (at t1) and directly after (at t2) water was added.

Labels	FLR1	FLR2	FLR3	FLR4	FLR5	FLR6	FLR7	FLR8	FLR9	FLR10
Start date	2012-03-08	2013-05-14	2013-05-22	2013-05-23	2013-05-14	2013-05-16	2013-05-16	2013-05-17	2013-05-17	2013-05-20
Pellet (upper part)										
w (%)	14.8	15.7	15.7	15.7	15.7	15.7	15.7	15.7	15.7	15.7
Actualt total mass mp,tot (g)	58.8	67.7	62.55	181.7	67.7	67.7	67.7	67.7	67.7	67.7
D (mm)	26	26	25	36	26	26	26	26	26	26
H (mm)	125	125	125	175	125	125	125	125	125	125
Dry density (kg/m3)	772	882	881	882	882	882	882	882	882	882
Degree of saturation (%)	16	20	20	20	20	20	20	20	20	20
Buffer (lower part)										
w (%)	19.2	21.6	26.9	22.65	21.6	21.6	21.6	21.6	21.6	21.6
Actual total mass mb,tot (g)	123.8	123.96	120.52	337.7	123.8	124.2	124	124.1	124.3	124.2
D (mm)	26	26	25	36	26	26	26	26	26	26
H (mm)	125	125	125	175	125	125	125	125	125	125
Dry density (kg/m3)	1565	1536	1548	1546	1534	1539	1537	1538	1540	1539
Degree of saturation (%)	69	74	94	79	74	74	74	74	75	74
Pellet and Buffer										
Average degree of saturation (%) at t1	36	42	49	43	42	42	42	42	42	42
Mass of water added (g)		39.8	39.9	103.8	42.6	41.5	44.0	42.9	42.7	46.5
Average degree of saturation (%) at t2		95	107	95	98	97	100	99	99	104

Water saturation and water supply

Initially a solution of 2 mM NaCl was added by evacuation of filters, tubes and devices. The salt content of the solutions was increased to 50 mM NaCl in all tubes in April/May 2014, i.e. after two years for FLR1 and after one year for FLR2–FLR10.

A constant water pressure of 70 kPa was introduced on 2015-10-05 in all devices, except FLR1 and FLR5, but already in September that year different water pressures between 0–100 kPa was used during shorter or longer time intervals. Regarding FLR1 a constant water pressure of 70 kPa was not introduced until 2016-01-15 and regarding FLR5 no water pressure was introduced before the dismantling.

Swelling pressure measurements

Swelling pressure is measured in four (FLR1–FLR4) of the ten set-ups but not FLR5. The evolution of swelling pressure during the first two years, measured in the set-up similar to the one used for FLR5, is shown in Figure 6-6. The values at the time of dismantling of FLR5, i.e. at the time corresponding to the total time of FLR5, are tabulated in Table 6-3. The evolution of swelling pressure from all four set-ups from start to July 2016 are shown in Appendix 5.

Table 6-3. Swelling pressure from set-up FLR2 with similar set-up as FLR5 at a time corresponding to the test period of FLR5.

Type	Distance mm	Swelling pressure kPa	Direction[1]	Label in Figure 5-6
Pellet	250	179	Axial	FLR2 pellet (axial)
Pellet	187.5	247	Radial	FLR2 pellet (radial)
Block	62.5	3381	Radial	FLR2 block (radial)
Block	0	6231	Axial	FLR2 block (axial)

[1] The swelling pressure is measured as radial and axial stresses.

For comparison, the corresponding values measured with the set-up FLR1 differed approximately ± 20 % from the values measured with the set up FLR2 (given in Table 6-3). The measured stresses from FLR1 and mentioned in the same order as given in Table 6-3, i.e. pellet(axial), pellet(radial), block(radial), axial (block), were approximately 163 kPa, 292 kPa, 3 192 kPa 5 127 kPa. Comparing these results, it is important to notice that rectangular shaped grooves were used in FLR1 while triangular ones were used in FLR2, and that the positions of the measurements of swelling pressure were slightly different in the two tests (in the set-up FLR1 the radially measurements were done 47.5 mm and 202.5 mm from the bottom but 62.5 mm and 187.5 mm in the set-up FLR2).

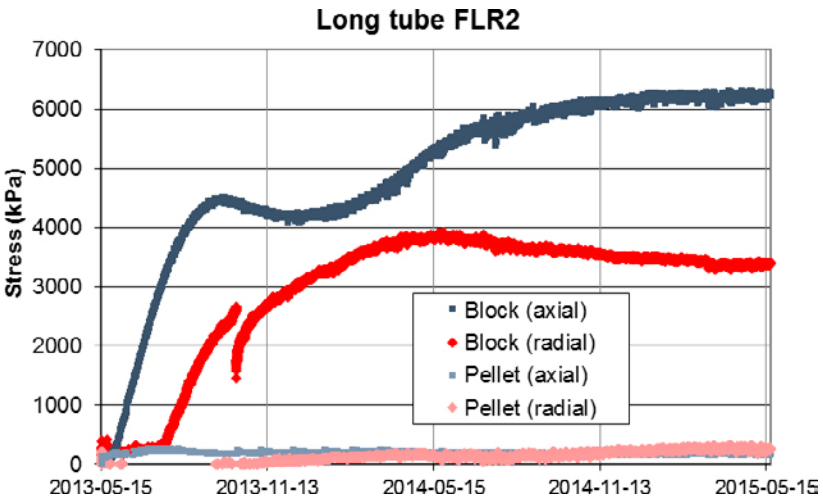

Figure 6-6. *Swelling pressure measured during the test period of FLR5 but measured on the equivalent set-up of FLR2.*

Termination, dismantling and sampling

The specimen FLR5 was terminated on 2015-05-20 as the first completed test of this test type. The filter at the upper piston and the plastic tubes were emptied from fluid by a peristaltic pump and the sample was forced upwards through the steel tube in one piece, Figure 6-7.

The sampling was made to provide information regarding

- if the buffer and pellet sections were saturated,
- the dry densities at the positions of the swelling pressure measurements,
- the distribution of dry density over the 250 mm specimen, with good resolution.

The first two bullet points were determined from samples 1–6 as shown in Figure 6-8, while the distribution was mainly determined from samples 7–10 further divided into smaller pieces used for determinations of water content only. In total, 38 water contents and 9 density determinations were made.

Figure 6-7. *The dismantled specimen FLR5.*

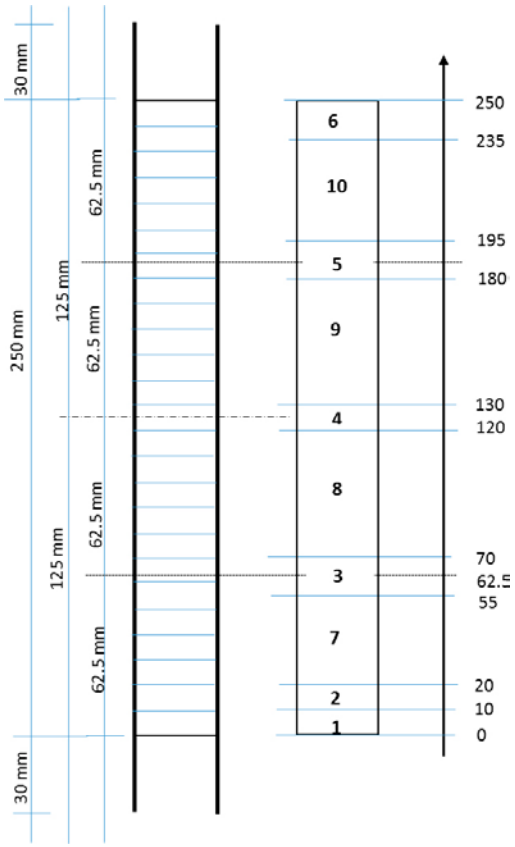

Figure 6-8. *The sampling scheme with a sketch of the tube with measures and lines indicating each 10 mm (to the left) and the dismantled specimen with the distance from the bottom to the top (to the right). The numbers (1–10) of the samples taken from the dismantled specimen are also given.*

Distribution of water content and density of FLR5

Both water content and density were determined on samples 1–6 from the FLR5 specimen and the results are presented in Table 6-4. The specimen was considered to be fully saturated although a low value of the degree of saturation is given for the uppermost sample.

Table 6-4. Results from samples 1 to 6 from FLR5. The distances from the bottom to the center of each sample are given with the thickness, water content, bulk density and dry density. In addition, the evaluated degree of saturation is given.

Sample ID	Distance mm	Thickness mm	Water content %	Bulk density kg/m^3	Degree of saturation %	Dry density kg/m^3
6	242.5	15	69.1	1434	84[1]	848
5	187.5	15	60.2	1675	101	1046
4	124.5	13	44.1	1856	106	1288
3	60.5	15	32.2	1952	101	1476
2	15	10	27.1	2017	100	1588
1	5	10	27.3	2018	101	1585

[1] This low value is not probable, see Figure 6-9 and Figure 6-10.

The distributions of water content and dry density over the specimen length are shown in Figure 6-9. In the diagram to the left circles mark the values from samples 1 to 6 from Table 6-3. In the diagram to the right the dry densities shown are either based on measured values (*Dry density 1* and marked with diamonds) or based on measured water contents and an assumed degree of saturation of 100 % (*Dry density 2* and marked with circles). In the diagram to the right the initial distribution of dry density is also shown, calculated in two different ways. The calculations are based either on the condition at installation (labelled *initial volume*) or on the condition after swelling i.e. filling the volume (labelled *final volume*). The initial condition of the buffer corresponds to the compacted blocks and the initial condition of the pellets corresponds to the dry mass and the inner volume of the tube, i.e. diameter of 25 mm. All values are tabulated in Appendix 5.

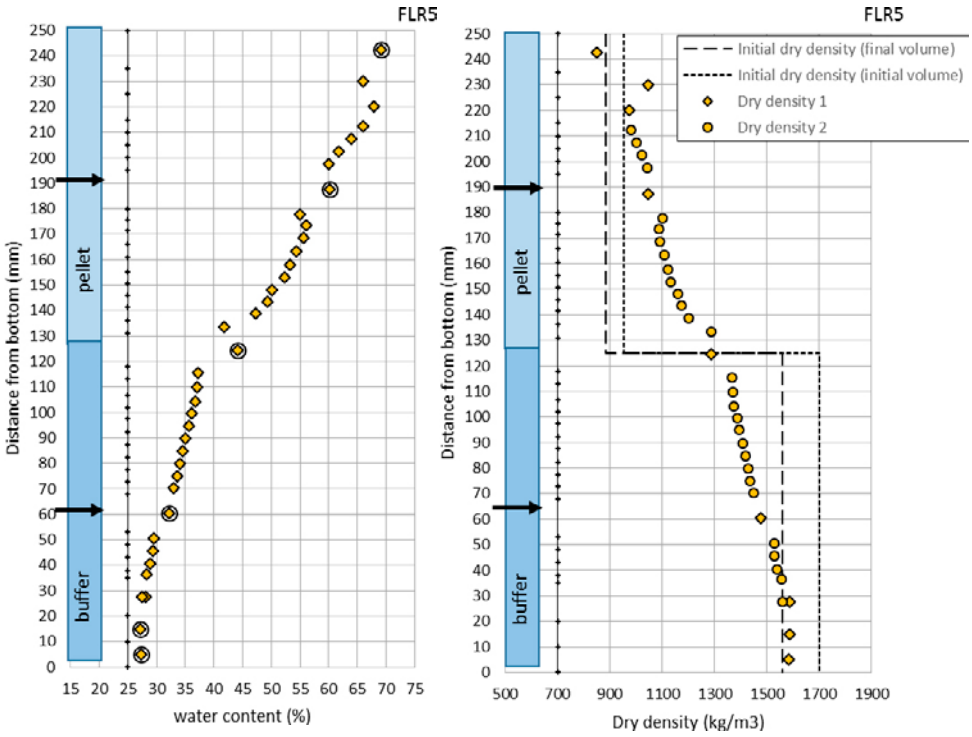

Figure 6-9. *Distribution of water content (to the left) and dry density (to the right) after dismantling of FLR5. To the left results from samples 1–6 are given with circles around. To the right the initial distribution of dry density, calculated both from the initial volume and the final volume, is given. At positions where both water content and bulk density were measured the Dry density 1 is calculated based on these while the Dry density 2 is calculated from the measured water content and an assumed degree of saturation of 100 %.*

Comments

For samples where both water content and bulk density were determined the degree of saturation was determined. Deviations from 100 % were noted in three samples, at the vertical distances 124 mm, 230 mm and 242.5 mm from the bottom. The deviations are considered to be caused by difficulties to take representative samples, i.e. the homogenisation is not fully achieved at the scale of sampling. In Figure 6-10 the results from the right of Figure 6-9 are shown again and the uppermost dry densities are re-calculated from the water content and 100 % degree of saturation, i.e. in the same way as Density 2 (circles). In addition, a best fit line of the measured final dry density between 27 mm and 220 mm are shown. In Figure 6-11 the swelling pressure from FLR2, see Table 6-3, are shown with the dry densities at the positions of the sensors from Table 6-4, however, the re-calculated dry density, i.e. Density 2 is used, at the uppermost position at 242.5 mm.

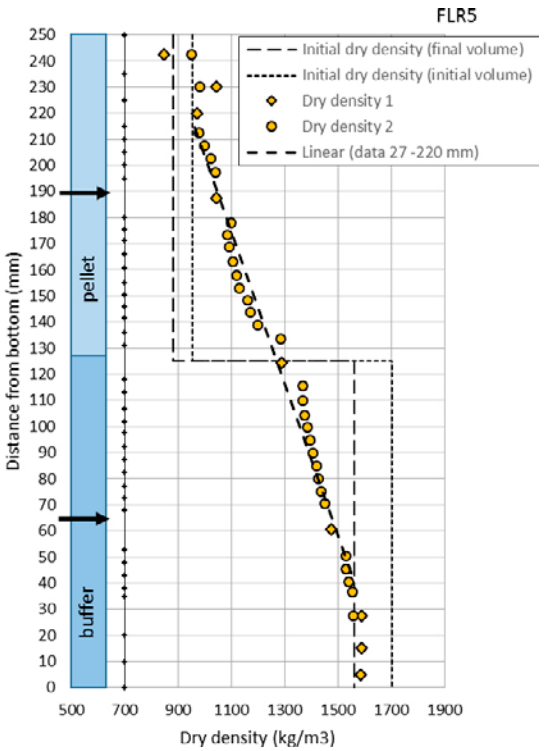

Figure 6-10. *Distribution of dry density, from Figure 6-9. The uppermost dry densities are given both as Dry density 1 (calculated from measured water content and density) and Dry density 2 (calculated from water content and an assumption of 100 % saturation). A best fit line for final dry densities between 27 mm and 220 mm are also shown.*

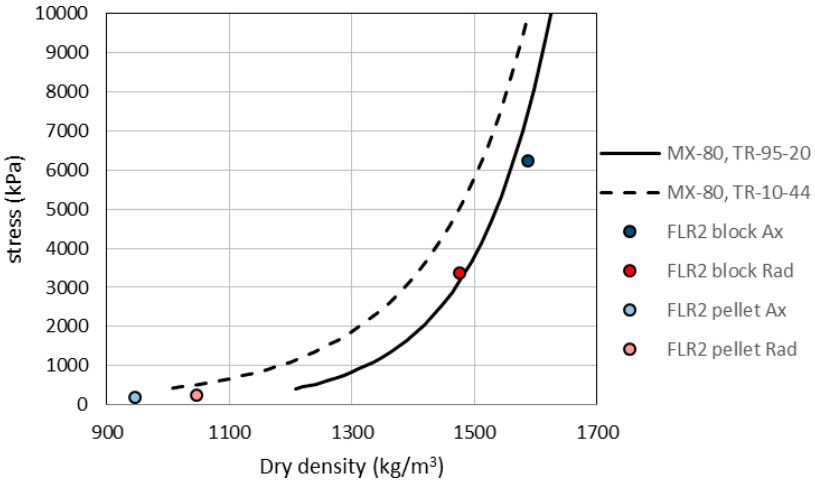

Figure 6-11. *Swelling pressure as a function of dry density. Results from FLR2 and FLR5 plotted with models presented by Börgesson et al. (1995) and Åkesson et al. (2010).*

7 Final comments

The present status report is a compilation of laboratory test results from a project on homogenisation tests of bentonite. The main purpose of the status report is to account for results derived up to July 2016 and to provide results that can be used for modelling some well-defined benchmark tests in order to improve the models or determine mechanical parameters for thermo-hydro-mechanical modelling of the behaviour of the bentonite buffer. Further analysis of the tests, test conditions, test results and limitations of the results will be made later in the project.

The objectives of the tests and the report have been well fulfilled:

- The tests and the results derived up to July 2016 have been presented in detail.
- The knowledge of the homogenisation process has been further increased.
- The results of many of the tests have been used as modelling tasks in the TF EBF (Task Force on Engineered Barrier systems)
  - the fundamental swelling tests (both the basic and the high resolution, tests) have been used for checking and improving material models and evaluate the modelling results,
  - the friction tests have been used for the contact parameters,
  - the self-healing tests have been used for modelling and checking the ability to model complicated geometries.
- The long tube tests have been used for both analytical and numerical modelling in order to improve the knowledge of the effect of friction for limiting the homogenisation.

The results and analyses of these modelling efforts and comparisons with measuring results will be treated in a coming report.

References

SKB's (Svensk Kärnbränslehantering AB) publications can be found at www.skb.se/publications.

Börgesson L, Johannesson L-E, Sandén T, Hernelind J, 1995. Modelling of the physical behaviour of water saturated clay barriers. Laboratory tests, material models and finite element application. SKB TR 95-20, Svensk Kärnbränslehantering AB.

Dueck A, Goudarzi R, Börgesson L, 2011. Buffer homogenisation, status report. SKB TR-12-02, Svensk Kärnbränslehantering AB.

Dueck A, Goudarzi R, Börgesson L, 2014. Buffer homogenisation, status report 2. SKB TR-14-25, Svensk Kärnbränslehantering AB.

Dueck A, Goudarzi R, Börgesson L, 2016. Buffer homogenisation. Status report 3. SKB TR-16-04, Svensk Kärnbränslehantering AB.

Johannesson L-E, 2014. KBS-3H. Manufacturing of buffer and filling components for the Multi Purpose Test. SKB P-14-07, Svensk Kärnbränslehantering AB.

Karnland O, Olsson S, Nilsson U, 2006. Mineralogy and sealing properties of various bentonites and smectite-rich clay materials. SKB TR-06-30, Svensk Kärnbränslehantering AB.

Svensson D, Dueck A, Nilsson U, Olsson S, Sandén T, Lydmark S, Jägerwall S, Pedersen K, Hansen S, 2011. Alternative buffer material. Status of the ongoing laboratory investigation of reference materials and test package 1. SKB TR-11-06, Svensk Kärnbränslehantering AB.

Åkesson M, Börgesson L, Kristensson O, 2010. SR-site Data report. THM modelling of buffer, backfill and other system components. SKB TR-10-44, Svensk Kärnbränslehantering AB.

Appendix 1

Basic variables and swelling pressure from the HR-series

In the tables the final values of the basic variables (water content w, dry density ρ_d, degree of saturation S_r) and the swelling pressure (axial stress P_a, radial stress P_r) are given. The last column contains the total time for the swelling and homogenisation. In the table the positions 1, 2, 3 and 4 mean 15 mm, 30 mm, 45 mm and 60 mm, respectively from the bottom surface of the specimens and position 5 means at mid-height, i.e. 40 mm from the bottom. The abbreviation avr. means average over the specimen. The degree of saturation has been calculated with a particle density of ρ_s = 2 695 kg/m^3 for Calcigel, Chapter 3.

Table A1-1. Axial swelling. Results from test series HR-A.

		Initial values		Swelling		Final values			Swelling pressure		Total time
Sample ID	Material	w	ρ_d	$\rho_{d0}/\rho_{df} - 1$	pos.	w	ρ_{df}	S_r	Axial P_a	Radial P_r	
				%	mm	%	kg/m^3	%	kPa	kPa	Days
HR-A7	Calcigel	20	1 643	39	avr.	49.5	1 186	102	168	265	172
					1	40.3	1 308	102		524	
					2	41.4	1 292	103		273	
					3	54.4	1 101	101		195	
					4	66.2	977	102		69	
HR-A8	Calcigel	48	1 169	0[1]	avr.	45.4	1 246	103	154	197	129
					1	37.1	1 367	103		263	
					2	38.3	1 348	103		309	
					3	55.2	1 096	102		100	
					4	57.3	1 071	102		115	

[1] The specimen consists of two parts which filled the volume. The initial values are given as averages.

Table A1-2. Radial outward swelling. Results from test series HR-Ro.

		Initial values		Swelling		Final values			Swelling pressure		Total time
Sample ID	Material	w	ρ_d	$\rho_{d0}/\rho_{df} - 1$	pos.	w	ρ_{df}	S_r	Axial P_a	Radial P_r	
				%	mm	%	kg/m^3	%	kPa	kPa	Days
HR-Ro3	Calcigel	23	1 694	45	avr.	49.1	1 172	102	154	73	146
					5	47.1	1 204	102		73	

Table A1-3. Radial inward swelling. Results from test series HR-Ri.

Sample ID	Material	Initial values		Swelling		Final values			Swelling pressure		Total time
		w	ρ_d	$\rho_{d0}/\rho_{df} - 1$	pos.	w	ρ_{df}	S_r	Axial P_a	Radial P_r	
				%	mm	%	kg/m^3	%	kPa	kPa	days
HR-Ri2	Calcigel	22	1 691	33	avr.	46	1 228	105	283	102	153

Appendix 2

Results from measurement of friction in the Fr-series

The test results are presented as the evolution of swelling pressure with time (axial and radial stresses) and the evaluated friction angle as a function of deformation from test Fr2-2. Since the swelling pressure was measured both as radial stress and axial stress the friction angle has been determined from both stresses and the results are shown in separated diagrams below.

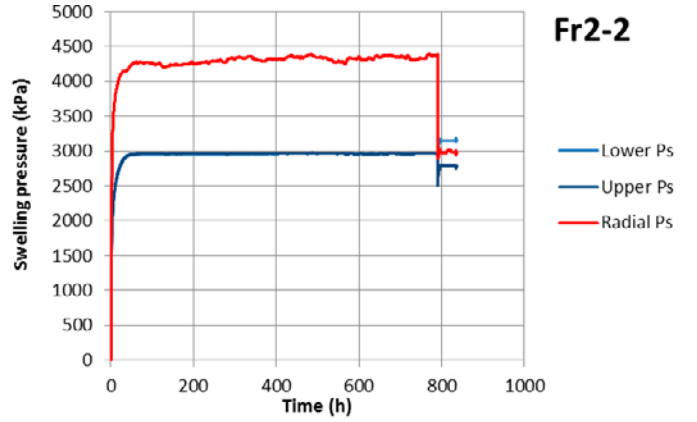

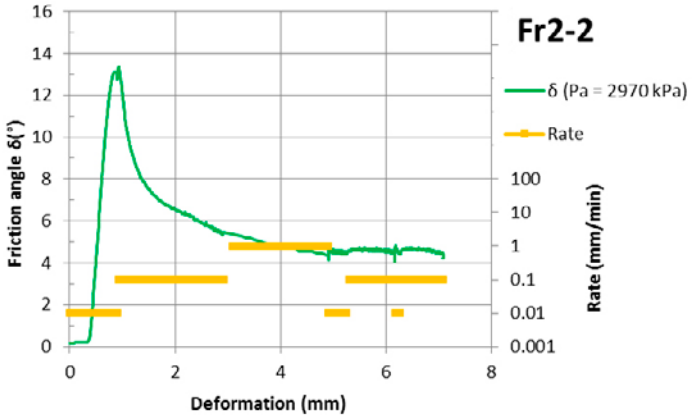

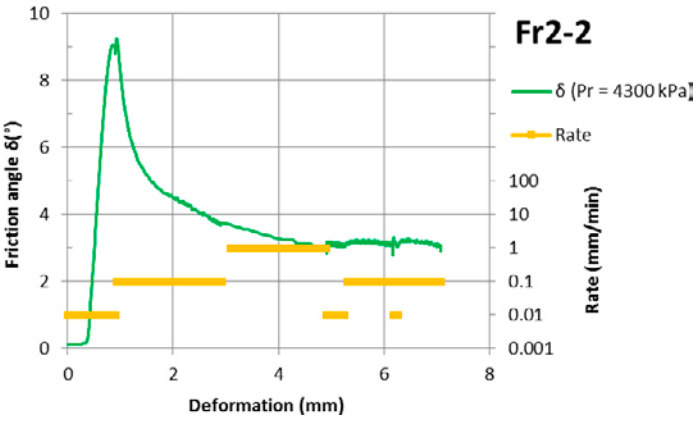

Appendix 3

Basic variables and swelling pressure from the W-series

Table A3-1. Initial conditions of the Wetting tests. Water was applied by circulation of 25 mM $CaCl_2$. The material Calcigel was used for the tests either as powder or as compacted specimens.

	Initial condition										Results at end of test					
Test ID	Lower part					Upper part							Swelling pressure measured			
	Specimen	H	D	w	Dry density	Specimen	H	D	w	Dry density	w	Dry density	As axial stress from part		As radial stress at	Total time
											Avr.	Avr.	Compacted	Powder	Mid-height	
		mm	mm	%	kg/m³		mm	mm	%	kg/m³	%	kg/m³	kPa	kPa	kPa	days
W1-2	Compacted	20	50	12.2	1 550	Powder	20	50	12.2	876	42.1	1 253	1 008	619		38
W1-3	Powder	20	50	12.2	876	Compacted	20	50	12.2	1 550	42.9	1 261	1 236	1 033	933	37
W1-4	Compacted	20	50	11.8	1 550	Powder	20	50	11.8	877	44.6	1 226	885	499	1 312	41
													955	587	1 045	64

Appendix 4

Results from the dismantled SH1

A4.1 Photos of the bentonite ring and equipment used

Figure A4-1. *Photo of cylinder ring with cavity used for test SH1.*

Figure A4-2. *Photos of the inner cylinder used for test SH1.*

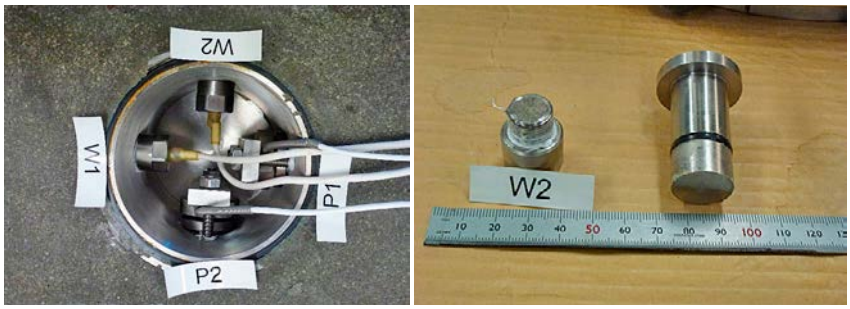

Figure A4-3. *Photos of the inner cylinder with attached sensors W1, W2, P1 and P2 (to the left) and of the casing used for the W2-thermocouple psychrometer and one of the pistons used for stress measurement P1 and P2 (to the right).*

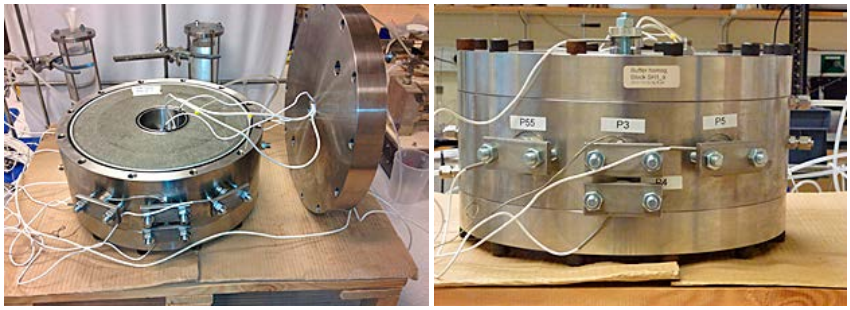

Figure A4-4. *Photo of the bentonite cylinder ring in place before the lid was put on at test start (left) and the device before lifting the lid at dismantling (right).*

Figure A4-5. *Photos of the bentonite ring after dismantling of SH1. The bentonite ring, still inside the steel device but without the inner steel ring, sawn radially and with the sampling marked on the upper surface (to the left) and the dismantled bentonite ring with the filter still left on the outer surface and the sampling marked on the bottom surface (to the right).*

A4.2 Timetable, start and end of test

Project	**Buffer homogenisation SH1**
Material	MX-80
Type of water	de-ionized
Dimension	
Diameter	D(outer) = 300 mm, D(inner) = 100 mm
Height	H = 100 mm
Gaps	Length = 70 mm (cirumferential)
	Height = 35 mm
	Depth = 50 mm
Estimated ingoing volume of water	
At start	380 ml
Including saturation of the bentonite	470 ml
Date	**Activity**
	Start of test
2012-11-26	Compaction of block to SH1.
2012-11-30	The block was machined with a drill and a rotating lathe.
2012-12-17	Sensors were mounted.
2012-12-18	The test started by applying water from the lower inlet and approximately 5 kPa.
2012-12-20	Water was flushed with 20 kPa for the first time.
2013-01-02	Water was flushed with 100 kPa for the first time.
2013-01-07	A constant water pressure of 100 kPa was applied.
	End of test
2015-08-14 15:30	The water pressure was lowered from 100 kPa to 0 kPa.
2015-08-19 08:45	The self healing test SH1 was terminated.
2015-08-19 09:45	The sensors were removed and the upper lid was opened.
2015-08-19 12:45	The bottom plate was removed.
2015-08-19 14:50	The block was dismantled and the outer filter separated from the block.
2015-08-19	The block was divided into two half circles. One was stored for later studies.
2015-08-20	Determination of water contents was completed.
2015-08-21	Density determinationwas completed.
2015-09-04	All sensors were controlled.

A4.3 Tabulated values of water content after dismantling

Table A4-1, Table A4-2 and Table A4-3 contain tabulated values of the water contents determined after dismantling of SH1 at the levels 1, 2 and 3, i.e. outermost, second outermost and innermost levels. The Sample ID contains information about the location of the samples and the last figure shows the level. The first part of the Sample ID shows the location of the sampling profile. The line denominations (L0, L20, L65, L85) indicate that the samples were taken along lines at specific angles (0°, 20°, 65°, 85°) from the center of the cavity. The sector denominations (A(2), A(1), B(2), B(1), C(2), C(1), D(2), D(1)) indicate that the samples were taken within the sector with continuous sampling between 0 and −45° from the center of the cavity. See section 5.3.

Table A4-1. Distribution of water content at level 1, i.e. outermost and towards the lid. For the samples from the lines, i.e. L0 to L85, the dry density was calculated from the water content and S_r = 100 %.

Sample ID	Distance mm	Water content %	Dry density kg/m³	Sample ID	Distance mm	Water content %	Dry density kg/m³
L0-1	12.5	26.2	1610	B(1)-1	12.5	26.5	1600
L0-1	32.5	26.8	1590	B(1)-1	32.5	27.3	1580
L0-1	47.5	27.5	1570	B(1)-1	47.5	27.8	1570
L0-1	62.5	28.6	1550	B(1)-1	62.5	28.8	1560
L0-1	77.5	29.9	1520	B(1)-1	77.5	30	1530
L0-1	92.5	30.9	1500	B(1)-1	92.5	31.5	1500
L20-1	12.5	26.2	1610	C(2)-1	12.5	26.5	1610
L20-1	32.5	27.3	1580	C(2)-1	32.5	27.1	1590
L20-1	47.5	27.6	1570	C(2)-1	47.5	27.5	1580
L20-1	62.5	28.2	1560	C(2)-1	62.5	27.9	1570
L20-1	77.5	29.2	1530	C(2)-1	77.5	28.8	1550
L20-1	92.5	30.6	1500	C(2)-1	92.5	30.5	1520
L65-1	12.5	25.3	1630	C(1)-1	12.5	26.5	1610
L65-1	32.5	25.7	1620	C(1)-1	32.5	27.1	1590
L65-1	47.5	26.1	1610	C(1)-1	47.5	27.5	1580
L65-1	62.5	26.2	1610	C(1)-1	62.5	28	1580
L65-1	77.5	26.8	1590	C(1)-1	77.5	28.4	1560
L65-1	92.5	28.3	1560	C(1)-1	92.5	30	1530
L85-1	12.5	25	1640	D(2)-1	12.5	25.9	1620
L85-1	32.5	25.6	1620	D(2)-1	32.5	27	1600
L85-1	47.5	25.8	1620	D(2)-1	47.5	26.7	1600
L85-1	62.5	26.1	1610	D(2)-1	62.5	27.2	1590
L85-1	77.5	26.5	1600	D(2)-1	77.5	27.4	1580
L85-1	92.5	28.3	1560	D(2)-1	92.5	29.4	1540
A(2)-1	12.5	26.7	1600	D(1)-1	12.5	25.9	1620
A(2)-1	32.5	27.5	1580	D(1)-1	32.5	27	1600
A(2)-1	47.5	28.4	1560	D(1)-1	47.5	26.7	1600
A(2)-1	62.5	29.8	1530	D(1)-1	62.5	26.9	1600
A(2)-1	77.5	31.2	1490	D(1)-1	77.5	27.5	1580
A(2)-1	92.5	33	1470	D(1)-1	92.5	28.8	1550
A(1)-1	12.5	26.7	1600				
A(1)-1	32.5	27.5	1580				
A(1)-1	47.5	28.4	1560				
A(1)-1	62.5	29.8	1530				
A(1)-1	77.5	31.2	1500				
A(1)-1	92.5	32.7	1470				
B(2)-1	12.5	26.5	1600				
B(2)-1	32.5	27.3	1580				
B(2)-1	47.5	27.8	1570				
B(2)-1	62.5	28.9	1550				
B(2)-1	77.5	30.3	1520				
B(2)-1	92.5	32	1480				

Table A4-2. Distribution of water content at level 2, i.e. the second outermost level. For the samples from the lines, i.e. L0 to L85, the dry density was calculated from the water content and S_r = 100 %.

Sample ID	Distance mm	Water content %	Dry density kg/m³
L0-2	12.5	26.7	1600
L0-2	32.5	27.5	1580
L0-2	47.5	29	1540
L0-2	62.5	30.7	1500
L0-2	77.5	32.2	1470
L0-2	92.5	31.9	1470
L20-2	12.5	27	1590
L20-2	32.5	27.8	1570
L20-2	47.5	28.3	1560
L20-2	62.5	29.6	1520
L20-2	77.5	30.7	1500
L20-2	92.5	32	1470
L65-2	12.5	25.9	1620
L65-2	32.5	26.5	1600
L65-2	47.5	26.5	1600
L65-2	62.5	26.7	1600
L65-2	77.5	27.2	1580
L65-2	92.5	28.7	1550
L85-2	12.5	25.6	1620
L85-2	32.5	26.1	1610
L85-2	47.5	26.3	1610
L85-2	62.5	26.5	1600
L85-2	77.5	26.9	1590
L85-2	92.5	28.7	1550
A(2)-2	12.5	27.2	1580
A(2)-2	32.5	28	1570
A(2)-2	47.5	29.9	1520
A(2)-2	62.5	31.7	1480
A(2)-2	77.5	33.1	1450
A(2)-2	92.5	34.1	1430
A(1)-2	12.5	27.2	1580
A(1)-2	32.5	28	1570
A(1)-2	47.5	29.9	1520
A(1)-2	62.5	31.8	1480
A(1)-2	77.5	32.8	1460
A(1)-2	92.5	34.2	1430
B(2)-2	12.5	26.9	1600
B(2)-2	32.5	27.7	1580
B(2)-2	47.5	28.7	1560
B(2)-2	62.5	31	1520
B(2)-2	77.5	32.4	1480
B(2)-2	92.5	33.7	1450
B(1)-2	12.5	26.9	1600
B(1)-2	32.5	27.7	1580
B(1)-2	47.5	28.7	1560
B(1)-2	62.5	29.8	1520
B(1)-2	77.5	30.8	1510
B(1)-2	92.5	32.8	1470
C(2)-2	12.5	26.9	1600
C(2)-2	32.5	27.5	1580
C(2)-2	47.5	27.7	1570
C(2)-2	62.5	28.5	1570
C(2)-2	77.5	29.8	1520
C(2)-2	92.5	31.4	1490
C(1)-2	12.5	26.9	1600
C(1)-2	32.5	27.5	1580
C(1)-2	47.5	27.7	1570
C(1)-2	62.5	28.3	1570
C(1)-2	77.5	29	1550
C(1)-2	92.5	30.4	1510
D(2)-2	12.5	26.4	1620
D(2)-2	32.5	26.8	1600
D(2)-2	47.5	27.1	1590
D(2)-2	62.5	27.9	1580
D(2)-2	77.5	28.5	1570
D(2)-2	92.5	30.1	1530
D(1)-2	12.5	26.4	1620
D(1)-2	32.5	26.8	1600
D(1)-2	47.5	27.1	1590
D(1)-2	62.5	27.5	1590
D(1)-2	77.5	28	1580
D(1)-2	92.5	29.4	1540

Table A4-3. Distribution of water content at level 3, i.e. innermost and at the cavity centre. For the samples from the lines, i.e. L0 to L85 the dry density was calculated from the water content and S_r = 100 %.

Sample ID	Distance mm	Water content %	Dry density kg/m³
L0-3	12.5	26.8	1590
L0-3	32.5	27.8	1570
L0-3	47.5	30.7	1500
L0-3	62.5	33.7	1430
L0-3	77.5	34.8	1410
L0-3	92.5	34.5	1420
L20-3	12.5	27	1590
L20-3	32.5	27.7	1570
L20-3	47.5	28.6	1550
L20-3	62.5	30.3	1510
L20-3	77.5	31.2	1490
L20-3	92.5	31.9	1470
L65-3	12.5	25.8	1620
L65-3	32.5	26.4	1600
L65-3	47.5	26.5	1600
L65-3	62.5	26.7	1600
L65-3	77.5	27	1590
L65-3	92.5	28.4	1550
L85-3	12.5	25.5	1630
L85-3	32.5	25.9	1620
L85-3	47.5	26.4	1600
L85-3	62.5	26.4	1600
L85-3	77.5	27	1590
L85-3	92.5	28.2	1560
A(2)-3	12.5	27.3	1590
A(2)-3	32.5	28.6	1560
A(2)-3	47.5	31.9	1480
A(2)-3	62.5	35.6	1400
A(2)-3	77.5	35.9	1400
A(2)-3	92.5	36.8	1390
A(1)-3	12.5	27.3	1590
A(1)-3	32.5	28.6	1560
A(1)-3	47.5	31.9	1480
A(1)-3	62.5	35.3	1400
A(1)-3	77.5	35.8	1410
A(1)-3	92.5	35.8	1400
B(2)-3	12.5	26.6	1600
B(2)-3	32.5	27.6	1580
B(2)-3	47.5	29.5	1530
B(2)-3	62.5	32.9	1460
B(2)-3	77.5	33.2	1450
B(2)-3	92.5	33.8	1440
B(1)-3	12.5	26.6	1600
B(1)-3	32.5	27.6	1580
B(1)-3	47.5	29.5	1530
B(1)-3	62.5	30.3	1520
B(1)-3	77.5	31.6	1490
B(1)-3	92.5	33.4	1460
C(2)-3	12.5	26.7	1600
C(2)-3	32.5	27.2	1590
C(2)-3	47.5	27.6	1580
C(2)-3	62.5	28.8	1560
C(2)-3	77.5	29.6	1530
C(2)-3	92.5	31	1500
C(1)-3	12.5	26.7	1600
C(1)-3	32.5	27.2	1590
C(1)-3	47.5	27.6	1580
C(1)-3	62.5	28.1	1570
C(1)-3	77.5	29	1540
C(1)-3	92.5	30.3	1520
D(2)-3	12.5	26.2	1610
D(2)-3	32.5	26.7	1600
D(2)-3	47.5	26.9	1600
D(2)-3	62.5	27.4	1590
D(2)-3	77.5	27.8	1580
D(2)-3	92.5	29.2	1540
D(1)-3	12.5	26.2	1610
D(1)-3	32.5	26.7	1600
D(1)-3	47.5	26.9	1600
D(1)-3	62.5	27	1590
D(1)-3	77.5	27.1	1590
D(1)-3	92.5	28.5	1550

Appendix 5

Results from the FLR-series

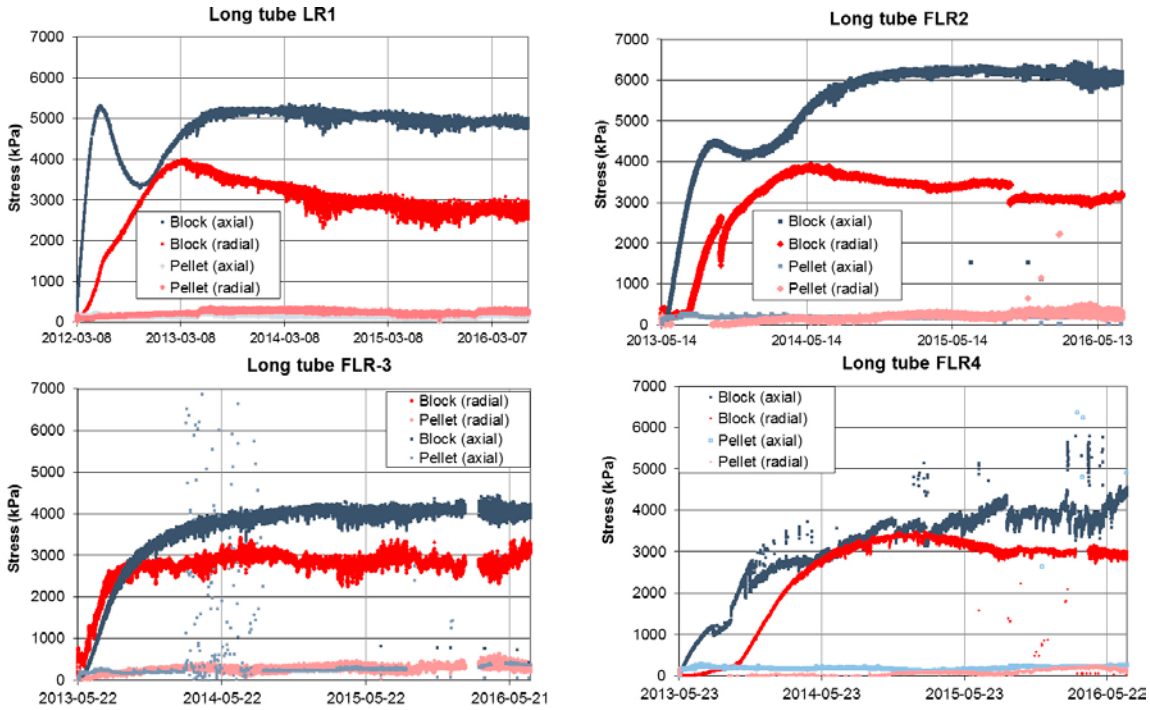

Figure A5-1. *Swelling pressure from start to 2016-07-01 from FLR1 to FLR4. Problems with sensors collecting data representing FLR3-pellet(axial) and FLR4-Block(radial) were detected and addressed during spring 2016, however all collected data are shown.*

Table A5-1. Timetable for FLR5.

Project	Buffer homogenisation				
	Long tubes				
Sample ID	**FLR-5**				
Information	**No sensors**				
	Equipment	Steel cylinder with triangular grooves			
	Sensors	0			
	Material	MX-80, five compacted specimens - lower half			
		MX-80 extruded pellet - upper half			
	Initial conditions		mass (g)	H (mm)	w (%)
		Compacted spec.	124	125	21.6
		Pellet	68	125	15.6
	Water	2 mM NaCl			
Date	**Activity**				
2013-05-14 14:00	Installtion of specimen.				
2013-05-15 14:00	Complete the installation.				
2013-05-15 13:58	Water added by evacuation of air in the system.				
	Circulation of water in upper piston on a regular basis.				
2014-04-17 09:20	Change concentration from 2mM to 50mM NaCl.				
	Circulation of water in upper piston on a regular basis.				
2015-05-20 09:00	End of test and dismantling.				

Table A5-2. Distribution of water content after dismantling of FLR5. The dry density is calculated from a measured water content and in case of Dry density 1 a measured bulk density and in case of Dry density 2 a degree of saturation Sr = 100 %.

Sample ID	Distance mm	Height mm	Water content %	Dry density 1 kg/m^3	Dry density 2 kg/m^3
6	242.5	15.0	69.1	848	
10-6	230.0	10.0	66.0	1045	
10-5	220.0	10.0	67.9	972	
10-4	212.5	5.0	66.1		980
10-3	207.5	5.0	64.0		1000
10-2	202.5	5.0	61.8		1023
10-1	197.5	5.0	60.1		1041
5	187.5	15.0	60.2	1046	
9-10	177.8	4.4	54.9		1100
9-9	173.5	4.3	56.0		1087
9-8	168.6	5.4	55.7		1091
9-7	163.3	5.3	54.3		1108
9-6	157.9	5.5	53.3		1120
9-5	152.9	4.5	52.4		1132
9-4	148.2	4.8	50.1		1161
9-3	143.7	4.3	49.3		1173
9-2	138.8	5.4	47.4		1200
9-1	133.6	5.1	41.7		1287
4	124.5	13.0	44.1	1288	
8-10	115.5	5.1	37.2		1367
8-9	109.8	6.2	37.1		1369
8-8	104.3	4.8	36.8		1375
8-7	99.7	4.4	36.1		1387
8-6	94.9	5.3	35.7		1396
8-5	89.8	4.8	35.1		1408
8-4	84.9	5.1	34.5		1419
8-3	79.8	5.0	34.1		1428
8-2	75.0	4.6	33.6		1438
8-1	70.4	4.7	33.0		1451
3	60.5	15.0	32.2	1476	
7-5	50.5	5.0	29.4		1529
7-4	45.5	5.0	29.4		1530
7-3	40.5	5.0	28.9		1541
7-2	36.5	5.0	28.3		1556
7-6 outer	27.5	15.0	28.1		1560
7-1 inner	27.5	15.0	27.5	1588	
2	15.0	10.0	27.1	1588	
1	5.0	10.0	27.3	1585	

Appendix 6

Samples and reports

The following tables show all tests presented in this report together with all results from TR-14-25 (Dueck et al. 2014) and TR-16-04 (Dueck et al. 2016). In addition some important tests from the report TR-02-12 (Dueck et al. 2011) are also mentioned.

The materials used, i.e. MX-80 or Calcigel, are mentioned in the tables below and for the tests presented in this report and in TR-16-04 the year of the delivery is also given; MX-80#2010[b], MX-80#2012, Calcigel#2006 or Calcigel#2014. The material MX-80#2010[b] was delivered before 2010.

Table A6-1. Tests made in the series A0 and mentioned in this report.

Sample ID	Material	Report
A01-09, A01-10	MX-80	TR-02-12
A01-12, A01-13	MX-80	TR-14-25
A01-14, A01,15, A01-16	MX-80#2010[b]	TR-16-04
A04-1, A04-2	Calcigel#2006	TR-16-04

Table A6-2. Tests made in the series R1 and mentioned in this report.

Sample ID	Material	Report
R11-10, R11-11	MX-80	TR-02-12
R11-17, R11-18, R11-19, R11-20, R11-21	MX-80	TR-14-25
R11-22, R11-23	MX-80#2010[b]	TR-16-04
R11-24	MX-80#2012	TR-16-04
R14-1, R14-2	Calcigel#2006	TR-16-04

Table A6-3. Tests made in the series R2 and mentioned in this report.

Sample ID	Material	Report
R21-09, R21-10, R21-11, R21-12	MX-80	TR-14-25
R21-13, R21-14	MX-80#2010[b]	TR-16-04
R24-1, R24-2	Calcigel#2006	TR-16-04

Table A6-4. All tests made in the series HR-A, HR-Ro, HR-Ri and HR-Iso.

Sample ID	Material	Report
HR-A1	MX-80	TR-14-25
HR-A2, HR-A3, HR-A4	MX-80#2010[b]	TR-16-04
HR-A6	Calcigel#2006	TR-16-04
HR-A7	Calcigel#2006	this report
HR-A8	Calcigel#2014	this report
HR-Ro1	MX-80	TR-14-25
HR-Ro2	Calcigel#2006	TR-16-04
HR-Ro3	Calcigel#2014	this report
HR-Ri1	MX-80#2010[b]	TR-16-04
HR-Ri2	Calcigel#2014	this report
HR-Iso	MX-80#2010[b]	TR-16-04

Table A6-5. All tests made in the series Fr.

Sample ID	Material	Report
Fr1-1 to Fr1-5, Fr1-7 to Fr1-9	MX-80	TR-14-25
Fr1-10, Fr1-12, Fr1-13	MX-80#2010[b]	TR-16-04
Fr1-11, Fr1-14	MX-80 pellet	TR-16-04
Fr1-15 to Fr1-17, Fr-19, Fr1-20	MX-80#2012	TR-16-04
Fr2-1	Calcigel#2006	TR-16-04
Fr2-2	Calcigel#2006	This report

Table A6-6. All tests made in the series W.

Sample ID	Material	Report
W1-2, W1-3, W1-4	Calcigel#2006	This report

Table A6-7. Two tests in the series SH.

Sample ID	Material	Report
SH1	MX-80#2012	TR-16-04 This report
SH2	MX-80#2012	TR-16-04

Table A6-7. All tests in the series FLR.

Sample ID	Material lower part	Material upper part	Report
FLR1–4 on going	MX-80#2012	MX-80 pellet#2011	This report
FLR5	MX-80#2012	MX-80 pellet#2011	This report
FLR6 to FLR10 on going	MX-80#2012	MX-80 pellet#2011	This report

Arkitektkopia AB, Bromma, 2019

SKB is responsible for managing spent nuclear fuel and radioactive waste produced by the Swedish nuclear power plants such that man and the environment are protected in the near and distant future.

skb.se